doi:10.1093/plcell/koaa028

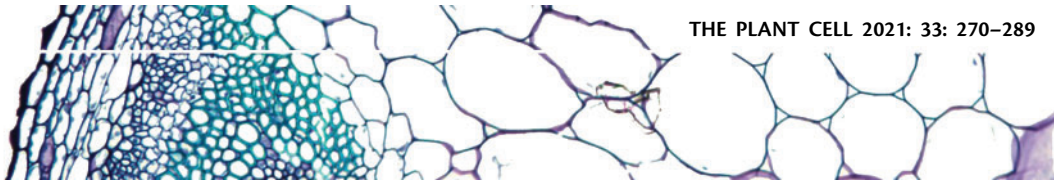

THE PLANT CELL 2021: 33: 270–289

Research Article

Enhanced nucleotide analysis enables the quantification of deoxynucleotides in plants and algae revealing connections between nucleoside and deoxynucleoside metabolism

Henryk Straube [1], **Markus Niehaus** [1], **Sarah Zwittian** [1], **Claus-Peter Witte** [1] and **Marco Herde** [1,*]

1 Department of Molecular Nutrition and Biochemistry of Plants, Leibniz Universität Hannover, Hannover 30419, Germany

*Author for correspondence: mherde@pflern.uni-hannover.de

H.S. and M.H. designed the study. H.S., M.N., S.Z., and M.H. acquired the experimental data. H.S. analyzed the data and H.S., C.-P.W., and M.H. interpreted the data. H.S., C.-P.W., and M.H. wrote the manuscript. All authors read and revised the manuscript and agreed on the final version.
The author responsible for distribution of materials integral to the findings presented in this article in accordance with the policy described in the Instructions for Authors (https://academic.oup.com/plcell) is: Marco Herde (mherde@pflern.uni-hannover.de).

Abstract

Detecting and quantifying low-abundance (deoxy)ribonucleotides and (deoxy)ribonucleosides in plants remains difficult; this is a major roadblock for the investigation of plant nucleotide (NT) metabolism. Here, we present a method that overcomes this limitation, allowing the detection of all deoxy- and ribonucleotides as well as the corresponding nucleosides from the same plant sample. The method is characterized by high sensitivity and robustness enabling the reproducible detection and absolute quantification of these metabolites even if they are of low abundance. Employing the new method, we analyzed *Arabidopsis thaliana* null mutants of *CYTIDINE DEAMINASE*, *GUANOSINE DEAMINASE*, and *NUCLEOSIDE HYDROLASE 1*, demonstrating that the deoxyribonucleotide (dNT) metabolism is intricately interwoven with the catabolism of ribonucleosides (rNs). In addition, we discovered a function of rN catabolic enzymes in the degradation of deoxyribonucleosides in vivo. We also determined the concentrations of dNTs in several mono- and dicotyledonous plants, a bryophyte, and three algae, revealing a correlation of GC to AT dNT ratios with genomic GC contents. This suggests a link between the genome and the metabolome previously discussed but not experimentally addressed. Together, these findings demonstrate the potential of this new method to provide insight into plant NT metabolism.

Introduction

Metabolomics of nucleotides (NTs) and nucleosides (Ns) in plants is a notably understudied area, in part is due to technical challenges concerning sample preparation and chromatographic separation. In particular, research on deoxyribonucleotide (dNT) and deoxyribonucleoside (dN) metabolism would greatly benefit from methods allowing the comprehensive quantification of these metabolite classes in plant samples.

Several enzymes of plant dNT metabolism have been functionally characterized in *Arabidopsis thaliana*, but a direct impact of loss-of-function mutants on the dNT pools

Received September 4, 2020. Accepted November 12, 2020. Advance access publication December 8, 2020

was hitherto only proven in one case with a PCR-based approach that allows only relative quantification of dNT triphosphates (dNTPs) in vivo (Wang and Liu, 2006; Garton et al., 2007; Yoo et al., 2009). Severe phenotypes like aberrant leaf morphology, growth inhibition, white spots in leaves, and reduced seed yield result from mutation of plant dNT metabolism genes (Wang and Liu, 2006; Garton et al., 2007; Dubois et al., 2011; Pedroza-García et al., 2015, 2019; Le Ret et al., 2018). Although not shown, these mutations likely cause altered cellular dNT concentrations, which in turn are probably often the reason for the phenotypic alterations. Changes of NT quantities affecting DNA and RNA replication were observed in similar mutants of non-plant organisms (Nick McElhinny et al., 2010a, 2010b; Gon et al., 2011; Kumar et al., 2011). Furthermore, the catalytic function of plant dN kinases could so far only be validated in vitro (Stasolla et al., 2003; Clausen et al., 2012; Pedroza-García et al., 2015; Le Ret et al., 2018; Pedroza-García et al., 2019), because possible changes of dN concentrations in the corresponding mutants cannot be assessed with current methods (Pedroza-García et al., 2015, 2019; Le Ret et al., 2018). The inability to detect dNs is also the reason why the metabolic fate of dNs is currently unknown in plants. dNs might be degraded by the same enzymes that also catabolize ribonucleosides (rNs), because at least some of these enzymes were shown to catabolize both types of substrates in vitro (Dahncke and Witte, 2013; Chen et al., 2016).

In contrast to ribonucleotides (rNTs), dNTs, and dNs, the detection and quantification of rNs and their degradation products is less challenging; this spurred a comprehensive characterization of the rN degradation pathways in vivo (Baccolini and Witte, 2019; Witte and Herde, 2020). The catabolism of rNs is integrated into a complex network including the de novo biosynthesis of rNTs and the salvage (recycling) of rNs and nucleobases ultimately giving rise to ratios and amounts of rNTs suitable for all downstream processes (Zrenner et al., 2006; Ashihara et al., 2020; Witte and Herde, 2020).

Unlike most animals, plants are able to fully catabolize purine and pyrimidine rNs including the nucleobases, using the released nitrogen for amino acid biosynthesis (Werner et al., 2010; Werner and Witte, 2011; Ashihara et al., 2020; Witte and Herde, 2020). Three key enzymes participate in the initial steps of rN catabolism: cytidine deaminase (CDA; Vincenzetti et al. 1999; Kafer and Thornburg, 2000; Chen et al., 2016; Witte and Herde, 2020), guanosine deaminase (GSDA; Dahncke and Witte, 2013; Witte and Herde, 2020), and nucleoside hydrolase 1 (NSH1; Jung et al., 2009, 2011; Baccolini and Witte, 2019; Witte and Herde, 2020). CDA was shown to deaminate cytidine and deoxycytidine in vitro and mutants of *CDA* accumulate cytidine in vivo (Chen et al., 2016). GSDA deaminates guanosine and deoxyguanosine in vitro and the mutants accumulate guanosine in vivo (Dahncke and Witte, 2013; Baccolini and Witte, 2019), while NSH1 participates in the hydrolysis of uridine, xanthosine, and inosine in vitro and in vivo (Jung et al., 2009; Riegler et al., 2011; Baccolini and Witte, 2019).

Mutants of *GSDA*, *CDA*, and *NSH1* show phenotypical abnormalities (Jung et al., 2011; Dahncke and Witte, 2013; Chen et al., 2016; Baccolini and Witte, 2019) during germination, development, and dark stress. The abnormal phenotypes are thought to result from the accumulation and toxicity of rNs or the lack of degradation-derived metabolites (Stasolla et al., 2003; Schroeder et al., 2018; Baccolini and Witte, 2019). So far, only metabolomic data for rNs and their degradation products have been obtained in *gsda*, *cda*, and *nsh1* mutants, whereas rNT, dNT, and dN pools have not been investigated due to technical limitations. However, it would be interesting to quantify dNs in these mutants to clarify whether the corresponding enzymes are indeed involved in dN degradation in vivo. The substantial accumulation of rNs (and perhaps also dNs) in these mutants might also result in altered concentrations of rNTs and dNTs because plants possess kinases for the salvage of rNs and dNs (Witte and Herde, 2020).

The primary metabolome comprises four main classes of metabolites: the amino acids, the carbohydrates, the lipids, and the NTs. While the first three classes are routinely characterized comprehensively in plant metabolome studies using well-established methods (Salem et al., 2020), this does not apply to NTs and NT-derived metabolites, which are often not analyzed at all or are highly underrepresented. A main reason lies in the lack of suitable methods for a comprehensive analysis of NTs in plant samples with modern mass spectrometry (MS) techniques. So far, NT analysis in plants (see literature survey summarized in Supplemental Table S1) have employed either liquid chromatography (LC) combined with photometric detection (Meyer and Wagner, 1985; Dutta et al., 1991; Katahira and Ashihara, 2006), a polymerase assay (Castroviejo et al., 1979; Feller et al., 1980; Wang and Liu, 2006; Garton et al., 2007), or thin-layer chromatography (TLC; Nygaard, 1972). These methods suffer from different drawbacks, for example, low sensitivity (photometric detection), relative quantification of only dNTPs (polymerase), or the need for radiolabelled starting material (TLC). Some metabolome studies quantified rNTs but not dNTs employing ion-exchange chromatography–MS or LC–MS (Rolletschek et al., 2011; Souza et al., 2015); however, recovery rates of these methods were not reported. To improve dNT detection, some protocols remove rNTs by a periodate treatment (Dutta et al., 1991) that likely also affects dNT species such as dGTP, which reacts with dicarbonyl compounds resulting from the addition of periodate (Tanaka et al., 1984; Henneré et al., 2003). Focused rN extraction methods from plant material also exist (Kopecná et al., 2013) but these are not suitable for NT species. Ideally, a method coupling LC with modern MS would be needed.

Plant samples are particularly challenging for metabolomics employing LC–MS because plants contain a plethora of metabolites making extracts (the matrix) very complex.

In fact, we previously quantified dNTPs in embryos of *Drosophila melanogaster* (Liu et al., 2019), but that same method failed to work for Arabidopsis tissues. So-called matrix effects can cause ion suppression greatly reducing the sensitivity of detection in the MS, which for dNTs is critical as they are not abundant in plant cells. Studies in human cells suggest that solid phase extraction (SPE), either employing a silica or an anion exchange resin, is uniquely suited to enrich NTs and reduce matrix effects for sensitive detection (Cohen et al., 2009; Pabst et al., 2010; Kong et al., 2018). Additionally, it has been pointed out that efficient quenching of enzymatic activities is essential to stabilize plant extracts, because they contain phosphatases displaying residual activity in mixed aqueous and organic solutions (Ullrich and Calvin, 1962; Bieleski, 1964; Ikuma and Tetley, 1976).

The LC of charged metabolites as front end for an MS analyzer is also not as straightforward as for moderately polar or hydrophobic compounds. For the LC–MS detection of NTs, various LC column materials have been used such as porous graphitized carbon in reverse-phase mode (Cohen et al., 2009) and resins carrying zwitterionic functional groups for hydrophilic interaction chromatography (Kong et al., 2018). A common problem with these chromatographies is that retention times can be unstable varying up to several minutes (Pabst et al., 2010). With the porous graphitized carbon stationary phase, this variation in chromatographic behavior is aggravated when crude plant extracts are used (our own observation) and might depend on the redox status of the column resin (Pabst et al., 2010). Taken together, these issues suggest that the detection and quantification of NTs in plant samples will require the development of a specially adapted protocol considering that methods of sample preparation and chromatography might interact to some extent.

In this study, we have established a sensitive and robust analytical method to simultaneously determine absolute concentrations of a comprehensive set of NTs and Ns in plants. The method works for a wide range of plant species including a moss (*Physcomitrium* [*Physcomitrella*] *patens*) and three algae (*Chlamydomonas reinhardtii*, *Mougeotia scalaris*, and *Volvox carteri*). We used the new protocol to analyze three Arabidopsis loss-of-function mutants in nucleoside catabolism lacking CDA, GSDA, and NSH1, respectively. We discovered that all three mutants harbor highly unbalanced rNTP and dNTP pools and we present evidence that CDA and NSH1 are not only required for rN but also for dN degradation in vivo.

Results

Optimization of sample preparation

The complex matrix of plant extracts notably complicates MS (Bieleski, 1964; Bieleski and Young, 1963; Nieman et al., 1978) preventing for example the straightforward detection of dNTs, which can be readily detected in non-plant samples (Kuskovsky et al., 2019). Additionally, plant samples must be efficiently quenched for NT analysis because plants possess stable phosphatases (Bieleski, 1964; Ikuma and Tetley, 1976) that are resistant to harsh conditions like organic solvents. A method (Figure 1) addressing these challenges was devised comprising tissue rupture and acid quenching, liquid/liquid extraction (LLE), weak anion SPE, and LC coupled to MS (LC–MS).

We evaluated different methods for sample preparation. In Table 1, we present the main findings of the optimization while the full detail of tested methods is shown in Supplemental Tables S2, S3. Consistent with previous studies, the NT triphosphates (NTPs) were more efficiently recovered upon extraction with strong acids like trichloroacetic acid (TCA) and perchloric acid (PCA) than with the organic solvent methanol (Bieleski, 1964; Dietmair et al., 2010) since the latter probably failed to inactivate all NT phosphatases. In our hands, recovery with PCA (Ashihara et al., 1987) was not as good as with TCA presumably because the PCA is removed by precipitation creating a bulky pellet, which traps liquid making quantitative sample recovery more difficult.

By contrast, TCA is removed by a LLE step in our method. Such a LLE has been developed over 40 years ago for mammalian systems (Khym, 1975) but has lost popularity, probably because the original protocol requires environmentally hazardous and expensive 1,1,2-trichlor-1,2,2-trifluorethan (Freon-113). We replaced Freon-113 with dichloromethane (DCM) and adopted the technology for plant extracts.

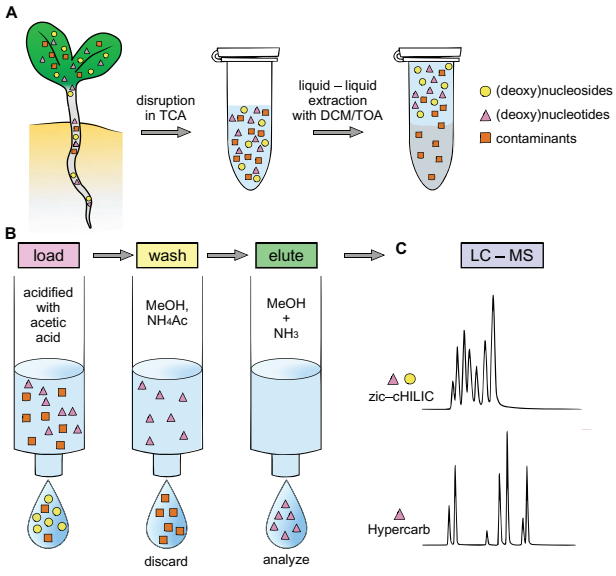

Figure 1 Schematic overview of the method for the extraction and analysis of NTs and Ns. Plant material is disrupted and quenched with TCA, which is removed together with apolar contaminants by LLE with DCM and TOA (A). The extract is loaded onto a weak-anion exchange SPE cartridge, the flow-through contains (deoxy)nucleosides for analysis. Subsequently, contaminants are depleted by washing with methanol (MeOH) and ammonium acetate (NH_4Ac), resulting in elution of (deoxy)ribonucleotides with MeOH and ammonia (NH_3; B). Isolated fractions are analyzed by LC–MS using a zic-cHILIC column (NTs and Ns) or a Hypercarb column (NTs; C).

Table 1 Selection of tested methods and their combined effect on NT recovery

Method	Quenching	LLE/acid quenching	Dilution	Recovery (%) dTTP	Recovery (%) ATP	Recovery (%) dTMP
3	80/20 MeOH/10 mM NH_4Ac pH 4.5 (v/v)	–	–	10.2	10.3	107.8
7	6% PCA	20% KOH	–	92.3	61.6	26.8
8	15% TCA	DCM/TOA (78/22 v/v)	–	89.6	92.7	44.9
9	15% TCA	DCM/TOA (78/22 v/v)	1 mL water	87.8	90.0	88.4

Apart from removing the TCA in an elegant way resulting in little sample loss, the LLE additionally eliminates apolar metabolites from the extract. This is advantageous because it reduces the complexity of the matrix likely contributing to the improved NT recovery in comparison to the PCA method. An additional boost of recovery for NT monophosphates (NMPs) was achieved by diluting the sample with water prior to application to the SPE (Tables 1, 2). The dilution results in a reduced salt concentration in the sample fostering the binding of the NMPs to the anion-exchange matrix of the SPE. One can envisage that by fine-tuning the salt load of the sample, it will be possible to select against NMPs and other less-strongly bound ionic compounds. Such a reduction of matrix complexity could be advantageous when for example only the NTPs are in the analytical focus.

Interestingly, in the flow-through of the SPE loading step, we were able to detect deoxy- and rNs (dNs). Therefore, we included Ns in the evaluation of the final method (Table 2) determining the recovery rate of NMPs and NTPs in the eluate as well as Ns in the flow-through. Recovery rates for NTPs ranged from 41.2% to 104.0%, for NMPs from 85.8% to 113%, and for Ns from 82.6% to 96.4% (Table 2). Dinucleotides were not assessed because we reasoned that they will co-elute with NMPs and NTPs. This was later confirmed for ADP. In summary, the data show that the new method allows the simultaneous extraction and preparation for MS detection of NTs and Ns from the same plant sample.

Table 2 Relative recovery of Ns, NMPs, and NTPs

Relative recovery (%)					
NTPs		NMPs		Ns	
dATP 15N	100.2				
dCTP 15N	104.0	dCMP 13C, 15N	113.1		
dGTP 13C, 15N	64.6				
dTTP 13C, 15N	87.8	dTMP 13C, 15N	88.4	Deoxythymidine 13C, 15N	94.8
ATP 2H	90.0	AMP 15N	90.2	Adenosine 13C	82.6
CTP 2H	102.5	CMP 13C, 15N	75.5	Cytidine 15N	96.3
GTP 2H	41.2	GMP 15N	85.8	Guanosine 15N	86.4
UTP 2H	91.0	UMP 15N	103.5	Uridine 15N	82.6
				Inosine 15N	96.4

Comparison of chromatography methods and method validation

The chromatography method has a substantial impact on the sensitivity of the MS analysis because analytes and matrix are differentially separated and focused by distinct chromatographic techniques. Ion chromatography and capillary electrophoresis as well as hydrophilic interaction chromatography (HILIC) and porous graphitized carbon (PGC) chromatography have been used as front ends for NT analysis by MS (Ashihara et al., 1987; Riondet et al., 2005; Pabst et al., 2010; Kong et al., 2018). We used a zic-cHILIC (Merck) for HILIC (in the following called the cHILIC method) and a Hypercarb column (Thermo) for PGC chromatography (in the following called the Hypercarb method) and optimized the respective chromatographic and MS parameters (see the "Materials and methods" section, Supplemental Figures S1–S3, and Supplemental Tables S4–S6). Using the Hypercarb method, a lower limit of quantitation (LLOQ) of 0.1 pmol on column for NTs was determined, which was 5–50 times lower than the 0.5–5 pmol LLOQ on column measured by the cHILIC method (Table 3). For Ns, the LLOQ was 0.1 pmol on column (Table 4). These sensitivities are similar or even better than those previously described for the analysis of NTPs from mammalian cells (Kong et al., 2018). Thus, the sensitivity of our method is sufficient to allow for the first time the detection and quantification of dNTs in plant material by MS.

The quantification of isotope standards (ISTDs) spiked into matrix derived from SPE and resolved either by the Hypercarb or cHILIC method showed that standard amount and detector signal correlated with good linearity resulting in R^2 values equal or higher than 0.96 for all tested substances (Tables 3, 4). Different physiological conditions leading to changing NT or nucleoside concentrations can therefore be investigated.

Intra- and inter-day precision was evaluated for all used chromatography methods and three different concentrations of ISTDs in plant matrix (Supplemental Tables S7, S8). In general, the coefficient of variation (CV%) was higher for the cHILIC than for the Hypercarb method and inter-day variation was higher than intra-day variation. The values ranged

Table 3 Calibration range, coefficient of determination (R^2), and LLOQ for NTPs using the Hypercarb or the cHILIC method

	Calibration range (pmol)	R^2 Hypercarb	Hypercarb LLOQ (pmol)	R^2 cHILIC	cHILIC LLOQ (pmol)
dATP	2.5–80	0.96	0.1	0.99	1
dCTP		0.98	0.1	0.99	1
dGTP		0.99	0.1	0.97	1
dTTP		0.99	0.1	0.98	0.5
ATP	25–800	0.99	0.1	0.98	1
CTP		0.96	0.1	0.98	1
GTP		0.99	0.1	0.99	5
UTP		0.99	0.1	0.98	1

Table 4 Calibration range, coefficient of determination (R^2), and LLOQ for Ns using the cHILIC method

	Calibration range (nmol)	R^2 cHILIC	cHILIC LLOQ (pmol)
Deoxythymidine	0.125–2	0.99	0.1
Adenosine		0.99	0.1
Cytosine		0.99	0.1
Guanosine		0.99	0.1
Inosine		0.99	0.1
Uridine		0.99	0.1

from 11% to 31% and are in good agreement with the variations determined for other SPE-based methods for NT analysis in non-plant organisms (Kong et al., 2018; Cohen et al., 2009).

In order to assess the effectiveness of the SPE method, we compared the matrix effect factor (MEF) of matrix obtained from the LLE step (before SPE) with the MEF of matrix obtained from the complete method (after SPE). The higher the MEF, the greater is the signal suppression by the respective matrix (see the "Materials and methods" section). Additionally, the comparison was made for both chromatographic techniques used, i.e. depending on whether the sample was separated via the Hypercarb or cHILIC method. Irrespective of the chromatography method, the SPE lowered the MEFs substantially and enabled the detection of several standards that were undetectable without SPE (Supplemental Tables S9, S10). Interestingly, the MEFs were generally lower when the samples were analyzed with the cHILIC method, showing that not only sample preparation but also the type of chromatography is important. For Ns, which are not retained by the SPE, the removal of charged metabolites from the matrix by the SPE nevertheless reduced the MEFs (Supplemental Table S10). The matrix after SPE even exerted a positive effect on sensitivity compared with buffer for some analytes (cytidine, inosine and uridine). Such ion enhancement effects have been reported previously (Zhou et al., 2017).

The robustness of the presented method, reflected in the LLOQs, variations, and MEFs, is equal to published SPE protocols for NT analysis of other organisms (Harmenberg et al., 1987; Cohen et al., 2009; Guo et al., 2013; Kong et al., 2018). Remarkably, for Ns, the method has a superior recovery and a similar MEF compared with SPE methods focusing exclusively on N analysis (Sawert et al., 1987; Farrow and Emery, 2012; Kopecná et al., 2013). Until now, the parallel quantification of Ns and NTs from plant samples was not possible—this robust method now allows this analysis and thus opens up new possibilities to investigate the NT metabolism of plants in greater depth.

For metabolite analysis, many laboratories have access to an LC system coupled with a photometric detector, whereas a MS detector is less common. Thus, it would be desirable that our sample preparation method also improves the photometric detection of NTs. After treating the samples with LLE alone, we were unable to detect any signals for NTs in the UV trace (at 254 nm) using the cHILIC method, but after SPE several peaks were detected (Supplemental Figure S4). For proof-of-concept, we showed that MS signals for the rNTs ATP, UTP, CTP, and GTP were associated with four of the photometric peaks. This demonstrates that the sample preparation via LLE and SPE improves NT detection also when a photometric detector is employed. However, in this case, it is recommendable to use other (non-MS-compatible) chromatographic separation techniques with increased resolution for NTs (see e.g. Meyer and Wagner, 1985). Our sample preparation method requires little plant material and allows inter alia the quantification of CTP and GTP in Arabidopsis leaves even without MS, which before has been difficult (Ashihara et al., 2020). Therefore, it might generally increase the sensitivity for NTs independent of the chosen detection method. Nonetheless, the analysis of less abundant NTs with photometric detection, for example dNTPs, would require significant upscaling.

dNTP pools in different plants are variable and correlate with the genomic GC content

We first applied the new method for the detection of NTs in the model plant *A. thaliana*. From as little as 100 mg of fresh material of either 7-day-old seedlings grown in liquid culture or leaves of 33-day-old plants grown on soil, not only all canonical rNTPs but also all of their dNTP counterparts were robustly detected (Figure 2, A and B). The concentrations of the rNTPs were in the nmol g^{-1} range, while dNTPs were 100- to 1000-fold less concentrated (Table 5). Data on the NTP contents in plants are scarce (Ashihara et al., 2020; Witte and Herde, 2020; Supplemental Table S1). However, our results on dNTPs are overall consistent with those from a previous study using radiolabelled plant cells and TLC (Nygaard, 1972). Because ATP and UTP are needed in higher amounts as energy carriers and for cell wall

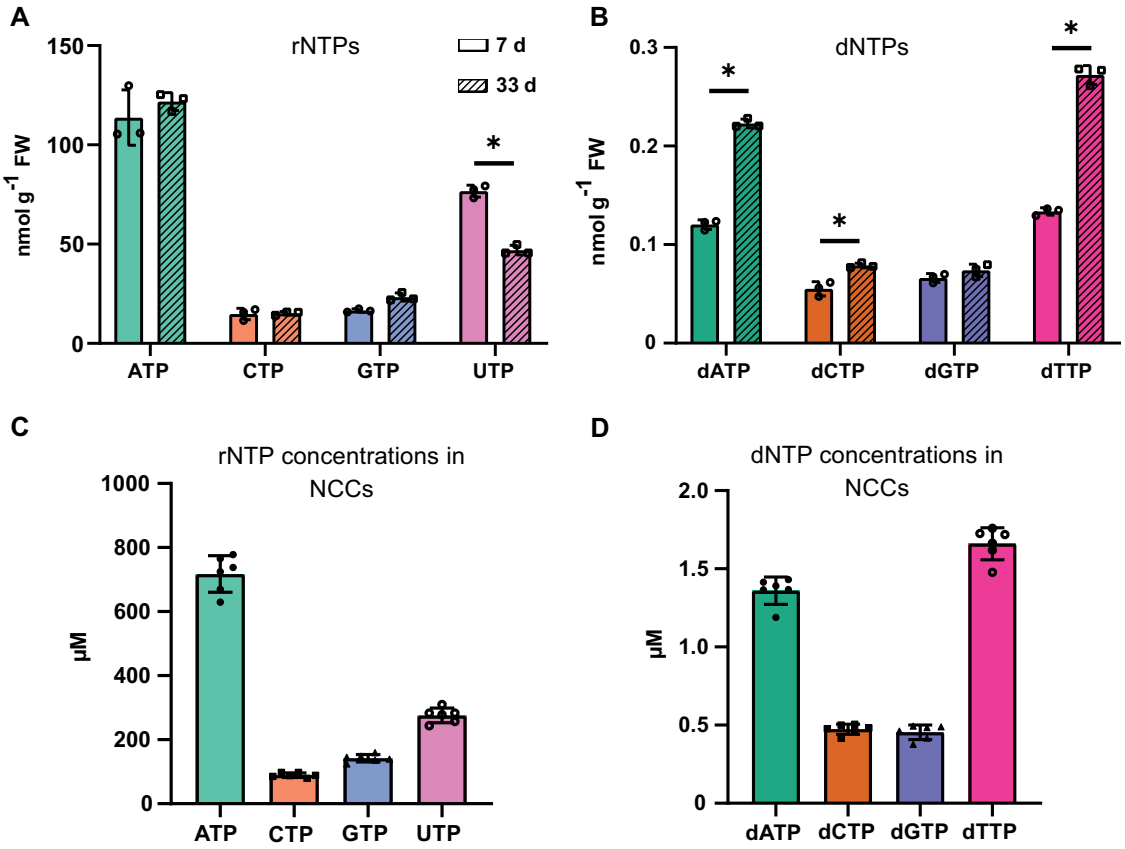

Figure 2 Cellular concentrations and absolute amounts of rNTs and dNTs in Arabidopsis leaves and seedlings. rNTs (rNTPs; A) and dNTs (dNTPs; B) were quantified in 7-day-old seedlings (unhatched bars) and 33-day-old rosette leaves (hatched bars). Each biological replicate represents a pool of several seedlings (A) or two leaves (B) which met the criteria outlined in the "Materials and methods" section from one individual plant. For seedlings, every replicate is a pool of seedlings grown together in one flask. Replicates were grown in parallel under identical conditions. Concentration of rNTPs (C) and dNTPs (D) in NT containing compartments of 33-day-old leaves. The concentration was calculated with the assumptions and formulas given in the "Materials and methods" section. Error bars indicate standard deviations (SD) for $n = 3$ biological replicates (A and B) or $n = 6$ biological replicates (C and D). * means $P < 0.05$ and was determined using a two-way ANOVA with Sidak's post test.

Table 5 Ratios of rNTP/dNTP in 7- and 33-day-old Arabidopsis plants

	ATP/dATP	CTP/dCTP	GTP/dGTP	UTP/dTTP
7 day	945	268	250	574
33 day	528	189	313	166

synthesis, respectively, the ratio of ATP/dATP and UTP/dTTP is higher than for CTP/dCTP and GTP/dGTP in seedlings (Table 5).

Interestingly, the dTTP and the dATP pools are increased and the UTP pool is decreased in older plants in comparison to seedlings (Figure 2, A and B). This may seem counterintuitive because one might expect more dNTPs in young growing tissue undergoing frequent cell divisions, but older tissues might require dNTPs for endoreduplication or for DNA damage repair. However, one needs to bear in mind that the growing conditions of the seedlings and the older plants were quite distinct, which may also account for the differences.

The immediate concentration of metabolites in a cell or cellular compartment influences enzyme activities or regulatory processes. It is therefore interesting to estimate the cellular concentrations of NTs. We used the cell and cell compartment volumes reported by Koffler et al. (2013) for leaves of 33-day-old plants. Based on the simplifying assumptions that NTs are equally distributed in the nucleus, cytoplasm, chloroplasts, and mitochondria, and largely absent from other cellular compartments, the average rNTP concentrations ranged from 100 to 750 µM whereas the concentrations of dNTPs were between 0.5 and 1.6 µM (Figure 2, C and D).

To ensure that the quenching in our method is suitable to preserve the phosphorylation status of the NTs, the adenylates (AMP, ADP, and ATP) in 33-day-old *A. thaliana* leaves were quantified (Table 6). The ratio of ATP/ADP was 15.2, while the ATP/AMP ratio was notably higher, resulting in an adenylate energy charge (AEC) of 0.97. We conclude that the phosphorylation status of these metabolites was maintained during the extraction, which is in line with the high recovery rates for these metabolites (Table 2). The ratios and the AEC are also consistent with results from other studies (Stitt et al., 1982; Guérard et al., 2011), although the

Table 6 Absolute amounts of AMP, ADP, and ATP from 33-day-old Arabidopsis plants grown under long day conditions

Metabolite	nmol g^{-1} FW[a]
AMP	0.4 ± 0.04
ADP	7.6 ± 2.2
ATP	115.6 ± 7.8
Ratios	
ATP/ADP ratio	15.2
ATP/AMP ratio	286.4
AEC[b]	0.97 ± 0.01

[a]n = 6 biological replicates, where every replicate represents the oldest leaves of a different plant.
[b]AEC is defined as (ATP + 1/2ADP)/(ATP + ADP + AMP).

ATP/ADP and ATP/AMP ratio in 33 day-old-plants is higher than in other studies for unknown (Stitt et al., 1982; Savitch et al., 2001; Carrari et al., 2005). Additionally, the data show that also ADP as an example for the dinucleotides is co-eluted with the NMPs and NTPs from the SPE and can be quantified with this method.

We also identified NTs using an Orbitrap mass analyzer coupled to the Hypercarb chromatography providing exact masses for precursor and product ions as well as isotope patterns as additional evidence for the correct identification of the metabolites. In samples of 7-day-old seedlings, we identified all canonical NTPs with high confidence by MS/MS (Supplemental Table S11) except dGTP and dCTP for which the detection was not sensitive enough. Several NTPs were also detected in full MS mode suggesting that the samples provided by our method are in principle suitable to perform non-targeted analysis.

Plant species differ greatly in their metabolite composition in part due to variation in secondary metabolism. We wanted to assess if our method established in Arabidopsis is suitable for dNTP quantification in samples from diverse plant backgrounds. We extracted dNTPs from 11 different species encompassing monocotyledons, dicotyledons, a bryophyte, and three algae. In all tested species, the sensitivity was sufficient to detect and quantify dNTPs (Supplemental Figure S5) proving that our method is generally suitable for NT analysis of plants.

Because in DNA G pairs with C and A pairs with T, one might assume that the ratios of the corresponding dNTPs, i.e. the dGTP/dCTP and the dATP/dTTP ratios, are (i) close to unity and (ii) similar in different plants. Consistent with this concept, the dGTP/dCTP ratios were similar in the investigated species (with the exception of *C. reinhardtii*) but were general slightly lower than one, however the dATP/dTTP ratios were more variable, with *Avena sativa*, *Oryza sativa*, and *Solanum lycopersicum* containing notably more dATP than dTTP and *P. patens* having more dTTP than dATP (Supplemental Figure S5 and Figure 3). We additionally asked whether species with a high GC content in the DNA also have proportionally more dGTP and dCTP in their dNTP pool (GC content in dNTPs). Our results show that there is a moderate to strong positive correlation between these two parameters with a R^2 value of 0.67 (Figure 4) suggesting a link between the genome composition and the dNTP metabolome.

CDA and NSH1 metabolize dNs in vivo

The role of several enzymes in rN degradation is already well established, but to date it remains unclear whether dNs are also substrates of these enzymes in vivo, probably because these compounds are rather difficult to detect and quantify. We chose to investigate null mutants of genes encoding CDA (Vincenzetti et al. 1999; Faivre-Nitschke et al., 1999; Kafer and Thornburg 2000; Chen et al., 2016), GSDA (Dahncke and Witte, 2013; Baccolini and Witte, 2019), and NSH1 (Jung et al., 2009, 2011; Riegler et al., 2011) to address this issue with our newly established method. GSDA deaminates the purine nucleoside guanosine to xanthosine and CDA deaminates the pyrimidine nucleoside cytidine to uridine. NSH1 hydrolyzes the glycosidic bond of uridine generating uracil and ribose and is as well an essential component of a nucleoside hydrolase complex required for the hydrolysis of xanthosine to xanthine and ribose (Figure 5).

In seeds and seedlings of the Arabidopsis wild type, all rNs including the low abundant inosine but also deoxyadenosine in seeds and deoxythymidine in seedlings were reliably detected (Supplemental Figure S6 and Figure 6). Relative and absolute abundances of rNs in the *GSDA*, *CDA*, and *NSH1* loss-of-function mutants and in wild-type plants (Supplemental Figure S6) were consistent with concentrations reported in previous studies using a different extraction approach (Chen et al., 2016; Baccolini and Witte, 2019). In all mutants the abundance of adenosine, a metabolite not investigated previously in the context of these mutants, was elevated in seedlings (but not in seeds) compared with the wild type. With respect to the dNs, seeds contained a pool of deoxyadenosine that was not affected by any of the investigated mutations (Figure 6). By contrast, seeds of the *nsh1* and *cda* mutants showed an accumulation of deoxythymidine not observed in the Col-0 or *gsda* backgrounds (Figure 6, A). In seedlings, deoxythymidine additionally accumulated in the *GSDA* mutant, but was also detected at a lower level in Col-0 (Figure 6, B). However, in both tissues, the *nsh1* mutant accumulated by far the most deoxythymidine, suggesting that NSH1 is directly involved in the turnover of this metabolite. High concentrations of guanosine and cytidine occurring in the *gsda* and *cda* mutants, respectively (Supplemental Figure S3), are probably inhibiting NSH1 partially (Witte and Herde, 2020), leading to the intermediate deoxythymidine build-up observed in these backgrounds. Furthermore, deoxycytidine accumulated exclusively in the *cda* mutant (Figure 6) providing evidence for a role of CDA in the catabolism of this dN.

In summary, we provide evidence that NSH1 is involved in deoxythymidine hydrolysis and that CDA is responsible for deoxycytidine deamination in vivo, consistent with the ability of CDA to deaminate this dN in vitro (Chen et al., 2016). GSDA deaminates deoxyguanosine in vitro (Dahncke and Witte, 2013), but intriguingly deoxyguanosine was not

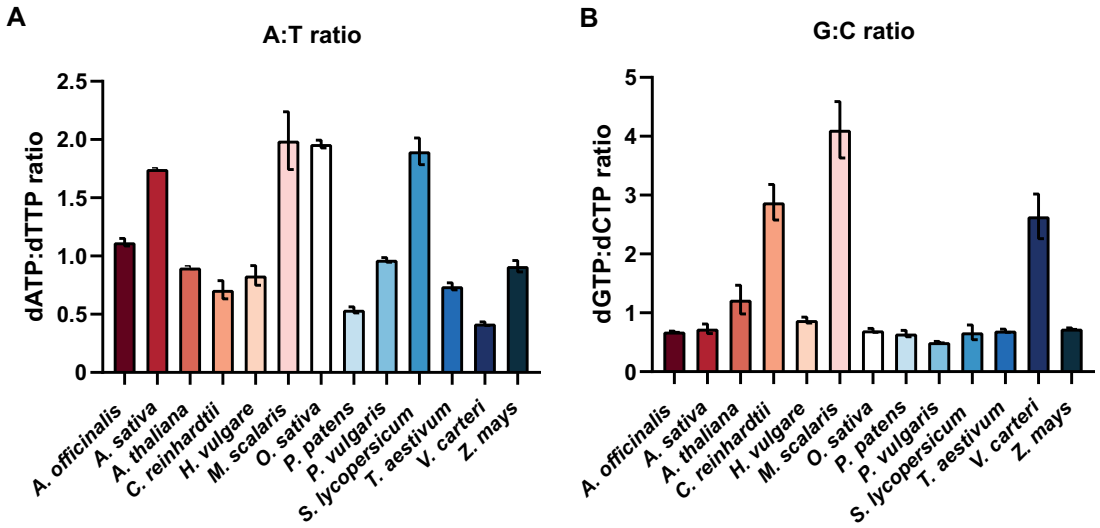

Figure 3 A/T and G/C ratios of dNTs (dNTPs) in different plant species. Ratios of dNTPs in *A. officinalis*, *A. sativa*, *A. thaliana*, *C. reinhardtii*, *H. vulgare*, *M. scalaris*, *O. sativa*, *P.* (*P.*) *patens*, *P. vulgaris*, *S. lycopersicum*, *T. aestivum*, *V. carteri*, and *Z. mays*. (A) Ratio of dATP to dTTP. (B) Ratio of dGTP to dCTP. Error bars indicate standard deviation (SD) for $n = 3$ biological replicates with each replicate representing a pool of several plants/seedlings all grown in parallel under the same environmental conditions.

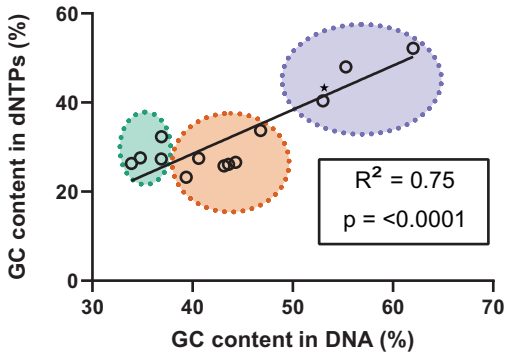

Figure 4 Regression analysis of the GC content in dNTPs and DNA. The GC content in the dNTPs (*y*-axis) is plotted against the genomic GC content (*x*-axis) and the Pearson correlation coefficient and the corresponding *P* value of a linear regression are calculated. Every white circle represents the average of three measurements. The green circle comprise all dicotyledonous species (*A. thaliana*, *P. vulgaris*, *S. lycopersicum*) and the bryophyte (*P. patens*), the orange circle encompasses the monocotyledonous species (*A. officinalis*, *A. sativa*, *H. vulgare*, *O. sativa*, *T. aestivum*, and *Z. mays*) and the purple circle alga (*C. reinhardtii*, *M. scalaris*, and *V. carteri*). * indicates an estimate of genomic GC content by extrapolation from known codon DNA sequences (R^2 without this datapoint is 0.73).

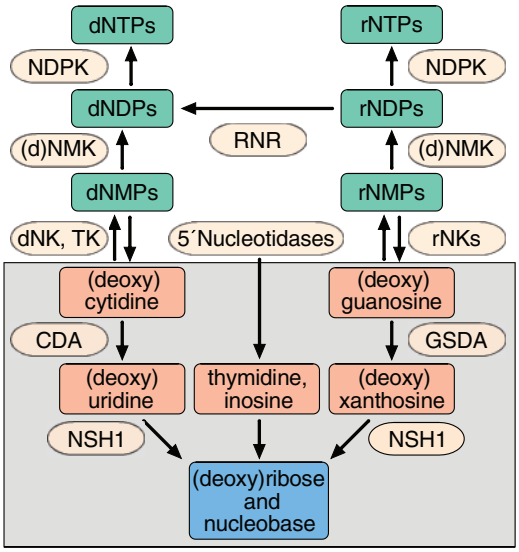

Figure 5 Scheme of nucleoside and NT metabolism. The (deoxy)nucleoside catabolism is highlighted with a gray background. NK, deoxynucleoside kinase; TK, thymidine kinase; rNK, ribonucleoside kinases; (d)NMK, (deoxy)nucleoside monophosphate kinases; and NDPK, nucleoside diphosphate kinases.

detectable in any of the analyzed genotypes (data not shown), although high concentrations of guanosine were detected in *gsda* seeds and seedlings (Supplemental Figure S6). Maybe for deoxyguanosine there is an additional metabolic escape route which is currently unknown.

CDA, GSDA, and NSH1 influence dNT and rNT pools

It is widely accepted that NT metabolism can be manipulated by the supply of extracellular Ns and nucleoside analogs, a concept exploited in chemotherapy (Galmarini et al., 2003; Robak and Robak, 2013). It is also established in plants that extracellular Ns can be taken up and interfere with plant metabolism (Traub et al., 2007; Chen et al., 2016; Ashihara et al., 2020). In plants, little is known about the impact of imbalanced intracellular N pools on the abundance of NTs. Therefore, we analyzed the NTs in the *cda*, *gsda*, and *nsh1* mutants, which have altered N pools. In seeds and seedlings lacking CDA and GSDA, the amounts of CTP and GTP are increased, respectively (Figure 7). Consistent with a previous study (Riegler et al., 2011), plants lacking NSH1

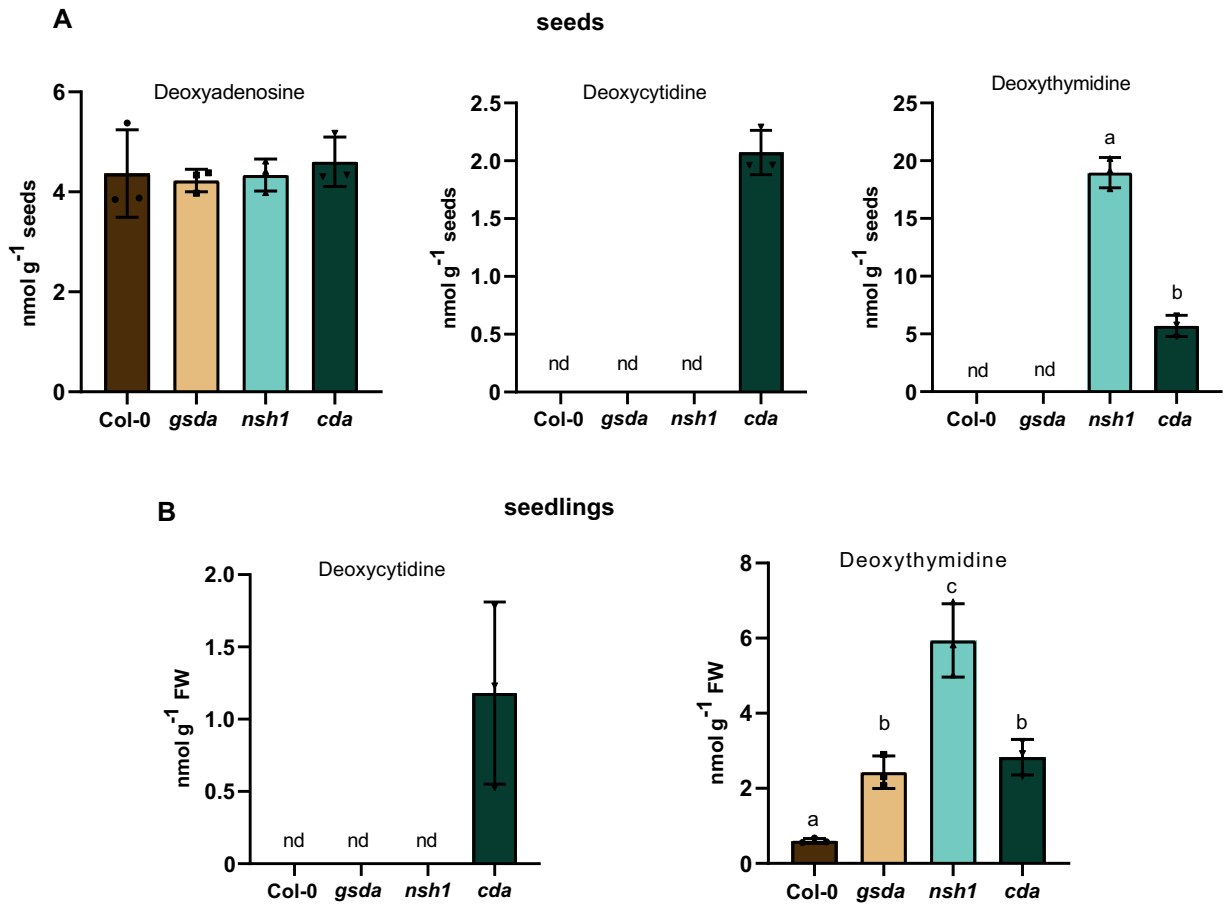

Figure 6 Absolute quantification of dNs in mutants impaired in the catabolism of rNs. Concentrations of dNs in seeds (A) and in 7-day-old seedlings (B) of *A. thaliana* wild type, as well as mutants in the degradation of purine and pyrimidine Ns (*gsda*, guanosin deaminase). Error bars are SD, $n = 3$ biological replicates, for seeds, three independent seed pools derived from different mother plants, for seedlings, three pools of seedlings from three independent liquid cultures were used. Statistical analysis was performed using one-way ANOVA with Tukey's post hoc test or in case of deoxythymidine by a two-tailed Student's *t* test. Different letters indicate $P < 0.05$. nd, not detected. FW, fresh weight.

accumulate more UMP and UTP compared with the wild-type (Figures 7, 8).

In general, the effects on NTP levels are also reflected by the respective NMPs (Figure 8). The accumulation of these NTs is probably a direct consequence of the increased pool sizes of the corresponding Ns (cytidine, guanosine, and uridine) in these mutants (Supplemental Figure S6), because the substrate availability for nucleoside and NT kinases (see scheme in Figure 5) is increased. However, some changes in the NT pools of the mutants cannot be explained by direct effects. The decrease of IMP concentrations in plants lacking GSDA or NSH1 (Figure 8, B) for example is puzzling because both contain much more inosine than the wild type (Supplemental Figure 3, B). Seeds and seedlings lacking GSDA have an increased content of ADP and ATP resulting in a higher AEC as well as more UMP and UTP. In *gsda* seedlings, there is also more CTP (Figures 7, 8). Thus, in seedlings, all measured NTP pools are strongly increased in the *gsda* background (Figure 7). The indirect changes in the *cda* and *nsh1* backgrounds are more subtle and are often similar. In seedlings, both mutants contain for example more GTP and ATP but in tendency less AMP than the wild type resulting in a higher AEC.

Except for the increased UTP level in *cda* seeds, all effects are more pronounced or even exclusively observed in seedlings compared with seeds. This also holds true for the Ns where for example adenosine only accumulates in mutant seedlings, but not in seeds (Supplemental Figure S6). As would be expected, these observations suggest that the flux through the NT metabolism is generally higher in growing seedlings compared with dormant seeds. Consistently, seeds harbor 5–10 times less rNTPs (and no detectable amounts of dNTPs), store adenylates mainly as AMP, display a lower ATP/ADP ratio, and have a lower AEC compared with seedlings which is in accordance with the literature (Raveneau et al., 2017; Figure 7).

Intriguingly, plants lacking enzymes of rN catabolism are not only impaired in the degradation of Ns (Figure 6 and Supplemental Figure S6) but also have elevated concentrations of dNTs, the substrates for DNA synthesis (Figure 9). The *CDA* mutant contains more dCTP similar to a human cancer cell line with reduced CDA activity (Chabosseau

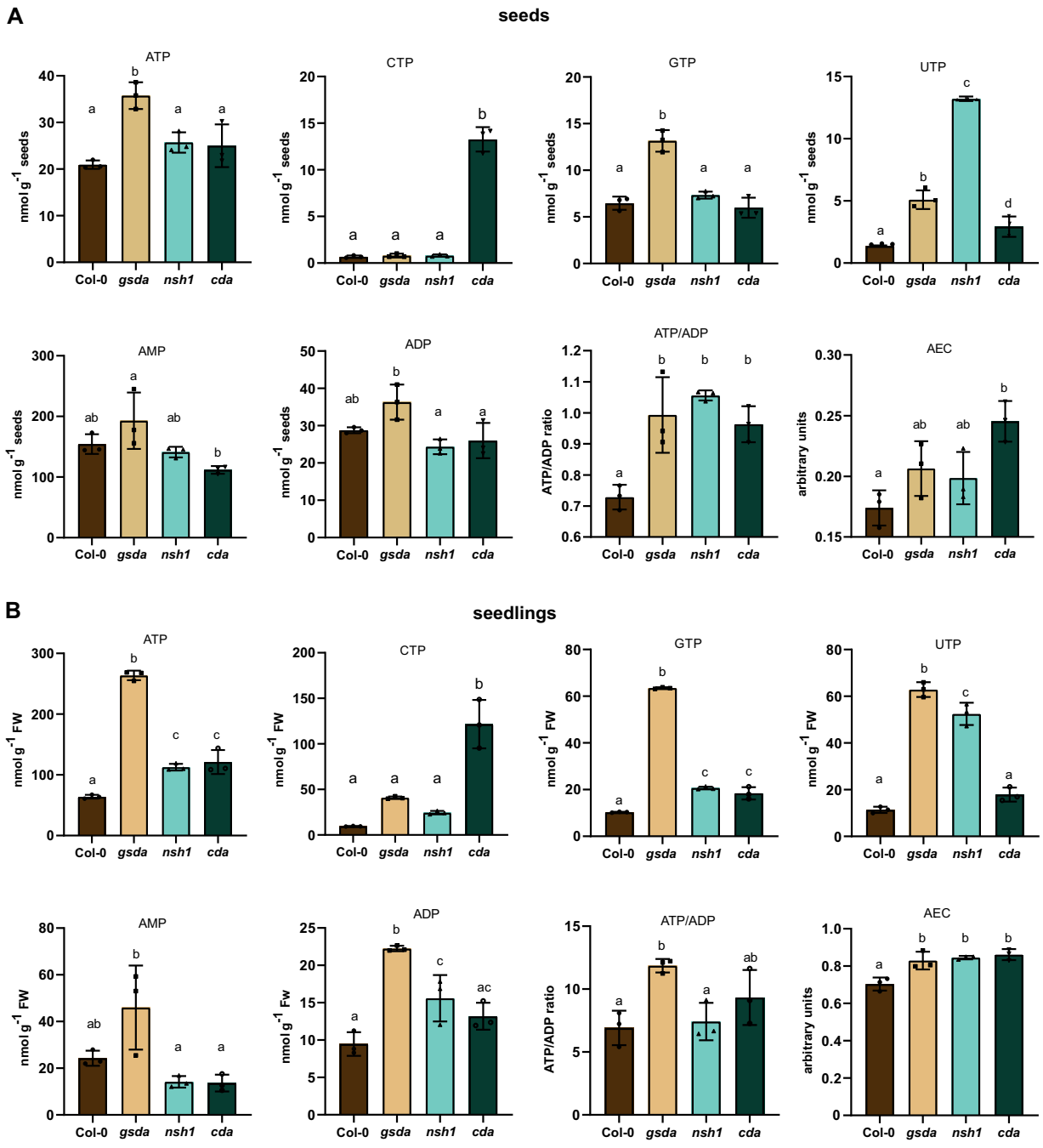

Figure 7 Comparison of the AEC, the ATP/ADP ratio, and the rNT concentrations between seeds and seedlings. Concentrations of rNTs, as well as ATP/ADP ratio and AEC in seeds (A) and in 7-day-old seedlings (B) of *A. thaliana* wild type, as well as mutants in the salvage and degradation of purine and pyrimidine Ns (*gsda*, guanosin deaminase) .Error bars are SD, $n = 3$ biological replicates, for seeds, three independent seed pools derived from different mother plants, for seedlings, three pools of seedlings from three independent liquid cultures were used. Statistical analysis was performed using one-way ANOVA with Tukey's post hoc test. Different letters indicate $P < 0.05$. FW, fresh weight.

et al., 2011). The high dCTP concentration may be a consequence of the high CTP concentration in *cda* seedlings. Interestingly, *gsda* seedlings accumulated the highest amounts of dGTP and dATP and also contained more dCTP and dTTP than the wild type. It seems as if the strongly elevated concentrations of ATP, GTP, and CTP in this mutant are mirrored in the corresponding dNTPs indicating that the pool sizes of these metabolites are directly linked. This also holds true for the higher dATP and dGTP concentrations mirroring the enlarged ATP and GTP pools in the *cda* and *nsh1* seedlings. In none of the mutants, deoxyguanosine was detected and deoxyadenosine concentrations were the same as in the wild type, whereas deoxycytidine was only found in *cda* background. It appears that the dN pool sizes of A,

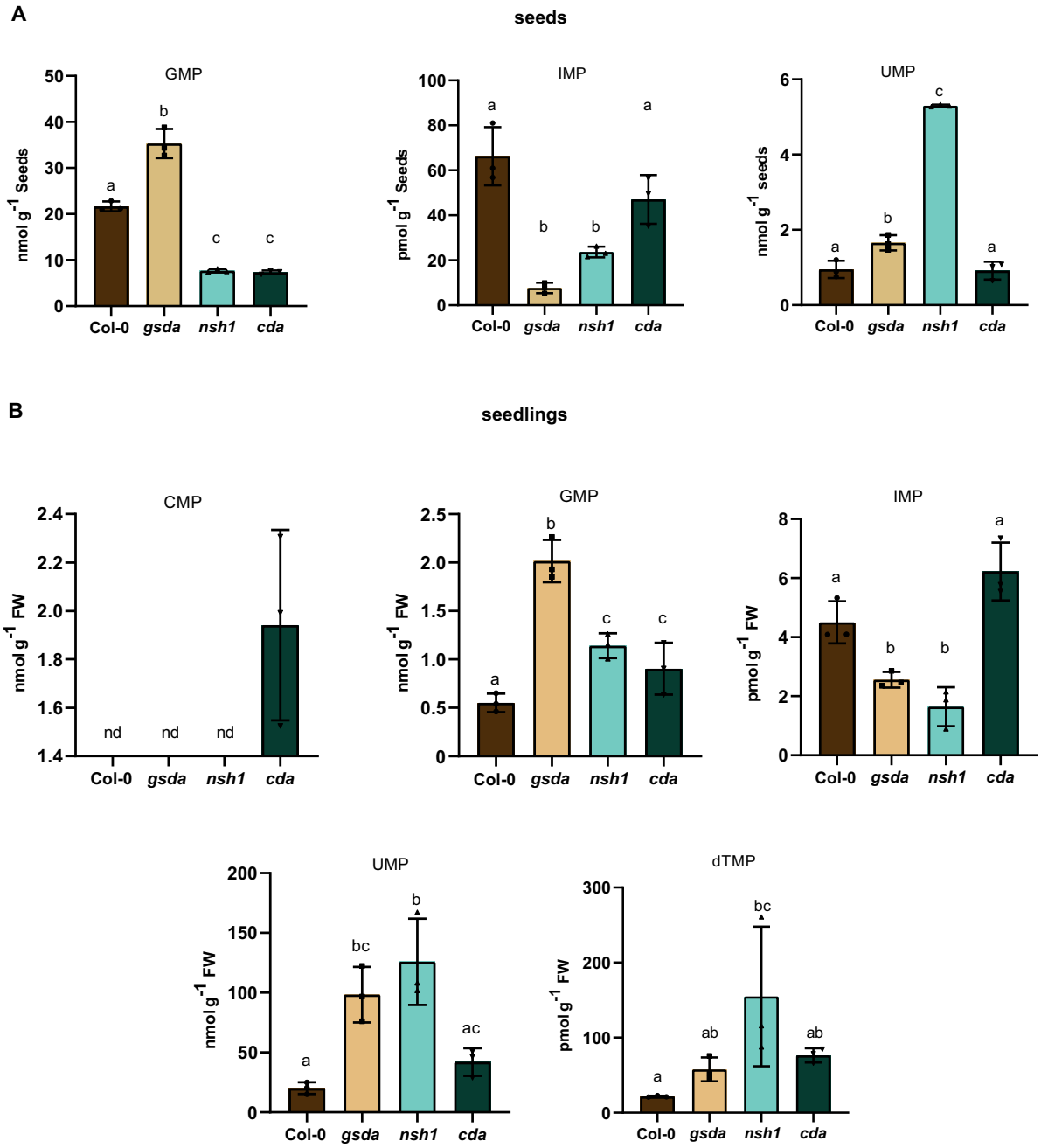

Figure 8 Absolute quantification of NMPs in seeds and seedlings of wild type and mutant plants impaired in nucleoside catabolism. Concentrations of NMPs in seeds (A) and in 7-day-old seedlings (B) of *A. thaliana* wild type, as well as mutants in the degradation of purine and pyrimidine Ns (*gsda*, guanosin deaminase) . Error bars are SD, $n = 3$ biological replicates, for seeds, three independent seed pools derived from different mother plants, for seedlings, three pools of seedlings from three independent liquid cultures were used. Statistical analysis was performed using one-way ANOVA with Tukey's post hoc test. Different letters indicate $P < 0.05$. nd, not detected. FW, fresh weight.

G, and C do not influence the corresponding dNTP amounts. By contrast, the deoxythymidine content seems to have a stronger influence on the dTTP pool size than the UTP concentration. Seedlings of the *cda* and the *gsda* mutants both have more deoxythymidine (Figure 6), more dTMP (Figure 8), and correspondingly more dTTP (Figure 9) than the wild type, but the UTP amounts are only elevated in the *gsda* and not in the *cda* background. However, the deoxythymidine and dTMP pools are largest in the *NSH1* mutant, but the dTTP concentration is only moderately increased, less than in *gsda* and *cda* seedlings. Although this seems contradictory, one needs to consider that uridine as well as deoxyuridine stemming from deoxycytidine deamination cannot be metabolized in *nsh1* background (uridine and resulting UMP accumulation are shown in Supplemental Figure S6 and Figure 8). The accumulation of

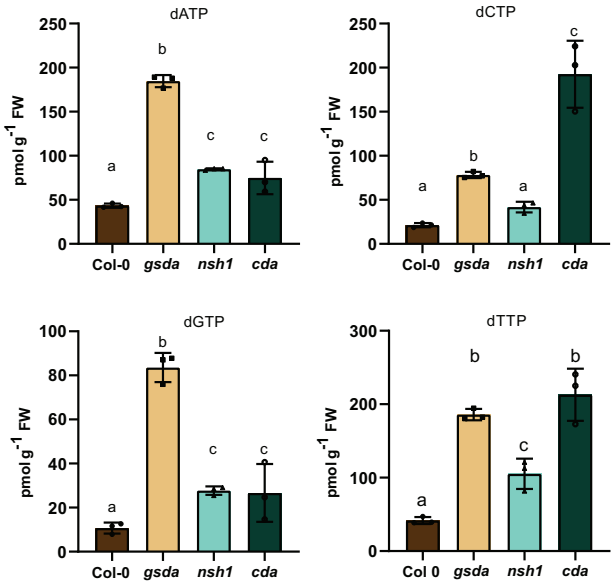

Figure 9 Absolute quantification of deoxynucleotide triphosphates in wild type and mutant seedlings impaired in nucleoside catabolism. Concentrations of dNTPs in 7-day-old seedlings of *A. thaliana* wild type, as well as mutants in the degradation of purine and pyrimidine Ns (*gsda*, guanosin deaminase). Error bars are SD, $n = 3$ biological replicates, for seedlings, three pools of seedlings from three independent liquid cultures were used. Statistical analysis was performed using one-way ANOVA with Tukey's post hoc test. Different letters indicate $P < 0.05$. FW, fresh weight.

these compounds may partially inhibit the thymidine kinases and maybe also thymidylate kinases known to be responsible for deoxythymidine (Clausen et al., 2012) and dTMP phosphorylation, respectively.

GSDA, CDA, and NSH1 were previously only considered to be involved in rN catabolism, but with our new method we can now show that they also play a role in dN degradation. By characterizing these mutants more in depth, we obtained a glimpse of the interconnection of deoxy- and rNT metabolism in plants. The data suggest that the ATP, GTP, and CTP pool sizes influence the amounts of dATP, dGTP, and dCTP, whereas the dTTP concentration seems to be more connected to the deoxythimidine than the UTP pool.

Discussion

A complex interplay of de novo synthesis, degradation, and salvage of rNTPs and dNTPs ensures that appropriate quantities of NTs are available for RNA and DNA synthesis as well as for signaling and energy metabolism (Zrenner et al., 2006; Witte and Herde, 2020). The fidelity of transcription and DNA replication is affected by altered ratios or changed total amounts of dNTPs (Nick McElhinny et al., 2010a, 2010b; Gon et al., 2011; Kumar et al., 2011; Buckland et al., 2014) emphasizing the importance of accurately balancing synthesis, degradation, and salvage of NTs and Ns. To gain a more comprehensive insight into these processes, a method allowing the parallel quantification of NTs and their respective Ns from one sample is a prerequisite. For the analysis of plants, such a method has not been available so far. Here, we fill this gap showing that the developed protocol is suitable for the analysis of NTs and Ns not only in seedlings and fully grown plants of Arabidopsis but also in a wide phylogenetic range of plants and even algae (Figure 2 and Supplemental Figure S5).

We found that the dGTP/dCTP ratios were quite similar between plant species, whereas the dATP/dTTP ratios (Figure 3) and the absolute contents of the dNTPs (Supplemental Figure S5) were more variable. Although clearly more evidence is needed, it is tempting to speculate that dNTPs produced in excess of their stoichiometric requirement in some plants might have an additional role in the respective species. The variation in dTTP contents for example might be related to the synthesis of dTDP-sugars and enzymes synthesizing dTDP-sugars are known to exist in plants (Neufeld, 1962; Frydman et al., 1963; Katan and Avigad, 1966).

Our data suggest that genome GC contents and the sum of dGTP and dCTP concentrations relative to all dNTPs are correlated (Figure 4). A dNTP-dependent evolution of the genomic GC content has been proposed (Vetsigian and Goldenfeld, 2008; Greilhuber et al., 2012; Šmarda et al., 2014) which may be an example of metabolism-driven evolution (de Lorenzo, 2014), but actually it is unknown if the dNTP abundances influence the DNA composition or vice versa. Certainly, more plant species need to be analyzed to test the validity of this correlation.

By analyzing well-characterized mutants of Arabidopsis impaired in rN catabolism (*nsh1*, *cda*, and *gsda*) with the new method, we obtained novel insights especially regarding the involvement of the corresponding enzymes in dN and dNT metabolism (Figures 6–9 and Supplemental Figure S6). We demonstrate that CDA and NSH1 partake in the catabolism of dNs in vivo (Supplemental Figure S3), showing that the known ability of CDA to deaminate deoxycytidine in vitro (Chen et al., 2016) is of relevance in the plant. Deoxythymidine accumulates in *nsh1* background suggesting that it is a NSH1 substrate in vivo, but so far this has not been investigated with the isolated enzyme in vitro.

The accumulation of dNs in seedlings of wild type and mutant plants indicates that even in this actively growing tissue some DNA or dNT degradation occurs (Figure 6). One needs to bear in mind that the dN accumulation in the mutants was observed despite the ability of the cells to salvage dNs. Salvage can strongly reduce accumulation as was shown for hypoxanthine which only accumulated when degradation and salvage were mutated (Baccolini and Witte, 2019). It is therefore possible that the flux through the dNs is much higher than one would assume from the relatively moderate levels of accumulation in the catabolic mutants. The origin of the dNs is currently unclear. They might be derived from DNA repair or from programmed cell death resulting in DNA degradation and release of dNMPs. Programmed cell death is a widespread process associated

with many aspects of plant development such as endosperm degradation, tracheary element differentiation, senescence, or microbial interactions (Aoyagi et al., 1998; Sakamoto and Takami, 2014). It was even suggested that plants store NTs and phosphate for embryogenesis and germination in the DNA synthesized by endoreduplication within the endosperm (Wang et al., 1998; Leiva-Neto et al., 2004; Lee et al., 2009). Another putative source of dNs might be the continuous house-keeping dephosphorylation of NTs. It was previously hypothesized that the phosphorylation status especially of dNTs may be constantly changed to control dNTP quantity and to improve their quality, i.e. to ensure that the dNTP pools only contain dNTs with canonical bases (Rampazzo et al., 2010; Leija et al., 2016). Because nucleoside and NT kinases best recognize their canonical targets, they may serve to purify the dNT pools if the pools are simultaneously subject to continuous dephosphorylation (Chen et al., 2018; Chen and Witte, 2020). It follows from this idea that dN salvage must be an essential process, because without it the dNTP pools would be depleted. In agreement with this concept, salvage by thymidine kinase 1a and 1b (Pedroza-García et al., 2015, 2019; Xu et al., 2015; Le Ret et al., 2018) is crucial for plant development since plants lacking functional copies of both corresponding genes have etiolated seedlings that need carbohydrate supplementation for survival (Xu et al., 2015).

There is no doubt that salvage of deoxythymidine is important, but here we provide evidence that plants also degrade this compound employing NSH1. This raises the question of how degradation and salvage are coordinated. Partially this might be achieved by spatial separation of both processes because at least Tk1b is located in the mitochondria and the chloroplasts whereas NSH1 and Tk1a are found in the cytosol (Jung et al., 2009; Xu et al., 2015), suggesting a preference for salvage in the organelles and a competition of both processes in the cytosol.

Intriguingly, compromising N catabolism leads not only to N accumulation but results in increased and imbalanced NT pools (Figures 7–9). The N and NT pools are interconnected by kinases (Ashihara et al., 2020; Witte and Herde, 2020; Figure 5), thus the most straightforward way to explain the increases in rNTP abundances is the higher availability of rN substrates for these enzymes. By contrast, higher amounts of dNTPs in the mutants are in most cases probably not a result of phosphorylation of dNs, because their pool sizes are often not increased except for deoxythymidine. Instead increased dNTP levels might result from greater reduction of rN diphosphates by rNT reductase (RNR; Nordlund and Reichard, 2006).

The current literature on plant NT metabolism suggests a temporal or spatial separation of synthesis, salvage, and degradation to avoid futile cycles (Ashihara et al., 2020; Witte and Herde, 2020). However, the concomitant occurrence in the catabolic mutants of increased amounts of Ns and of NTs, indicative of salvage and biosynthetic processes, suggests that a seedling can realize all these processes simultaneously. The enzymes for synthesis, degradation, and salvage might all be present in the same metabolic space but the flux through the respective pathways might be coordinated by the regulation of key enzymes. Being able to detect and quantify Ns and NTs is a prerequisite to investigate such hypotheses for example by using metabolic flux analysis and conditional mutants.

In the *gsda* mutant not only the direct substrate (guanosine) and its phosphorylated counterpart (GTP) accumulate but also ATP suggesting a crosstalk between these metabolites. It has been shown biochemically that GTP severely inhibits the activity of plant AMP deaminase, an enzyme that is involved in the regulation of guanylate synthesis, adenylate catabolism, and AEC regulation (Yabuki and Ashihara, 1991; Sabina et al., 2007; Witte and Herde, 2020). Sabina et al. (2007) could not detect an effect on GTP pools when feeding AMP deaminase inhibitors, but detected a two–fivefold increase of all adenylates, similar to the effects we observed in the *GSDA* mutant. This suggests that GTP accumulation in the *gsda* background (Figure 7) inhibits AMP deaminase in vivo, thereby raising ATP levels. Because IMP is the product of AMP deaminase, the inhibition of this enzyme might reduce IMP concentrations. That is precisely what we observed in the *gsda* seeds and seedlings (Figure 8). UTP and CTP levels were also raised in *gsda* plants probably to balance the elevated ATP and GTP concentrations. How pyrimidine and purine NT concentrations are kept in balance is currently unknown, but with our new method this interesting question could be further investigated.

Several phenotypes have been described for *gsda*, *nsh1*, and *cda* mutants such as delayed germination, compromised growth, and reduced recovery from dark treatment along with chlorosis (Chen et al., 2016; Schroeder et al., 2018; Baccolini and Witte, 2019). It has been suggested that these phenotypes are directly caused by the accumulation of rNs (Schroeder et al., 2018). However, here we show that NT pools are also disturbed in these mutants, which is known or is easily conceivable to cause detrimental effects. An increase in rNTP pool sizes for example leads to the undesired incorporation of rNTPs into human mtDNA (Nick McElhinny et al., 2010a, 2010b; Berglund et al., 2017). An elevated GTP concentration as observed in *gsda* seedlings might interfere with signaling processes in plants, in which GTP plays an important role (Assmann, 2002; Johnston et al., 2007). The biosynthesis of dNTPs by RNR will be disturbed by changed NTP pool sizes because RNR is stimulated by ATP and inhibited by dATP. Such pool size changes are known to lead to mutations and even to apoptosis in non-plant organisms (Kumar et al., 2011). Also in Arabidopsis, a mutant lacking a subunit of the RNR has disturbed dNTP levels and displays severe defects like sensitivity to UV-C light, DNA damage, developmental abnormalities, and cell death (Wang and Liu, 2006). Furthermore, it was shown that feeding deoxyadenosine to bean roots results in chromosomal breakage which was suggested to be a result of an increased dATP pool (Odmark and Kihlman, 1965).

In summary, it appears possible that the phenotypic alterations observed in the N catabolic mutants are at least partially caused by changed rNTP and dNTP pool sizes. It would be interesting to use these mutants to study the consequences of altered NT levels on transcriptional fidelity, DNA mutation rates, effects on the target of rapamycin (TOR) complex, and the involvement of dATP or ATP in plant immune signaling (Burdett et al., 2019; Nizam et al., 2019; Kazibwe et al., 2020).

NTs and Ns are not only involved in RNA and DNA metabolism but also play diverse roles for example in developmental processes and in plant pathogen interactions. The recently described *venosa4* mutant for example shows severe defects in chloroplast development and has a defect in an enzyme, which is likely involved in the dephosphorylation of dNTPs (Xu et al., 2020). In plant metabolome studies, NTs and Ns are strongly underrepresented hampering the discovery of novel functions for this major class of plant metabolites. The method described here will allow routine NT analysis to be performed in research focused on NT metabolism as well as in broad plant metabolomics surveys used in many plant research disciplines with the prospect of revealing so far unknown connections between the NT metabolome and other biological processes.

Materials and methods

Chemicals

Water, acetonitrile, methanol, ammonium acetate (all LC–MS grade), ethylenediaminetetraacetic acid (EDTA), and magnesium chloride were purchased from AppliChem. PCA and DCM were obtained from Carl Roth. 2′-Deoxyadenosine, 2′-deoxycytidine, 2′-deoxyguanosine, TCA, and trioctylamine (TOA) were purchased from Sigma–Aldrich. Twenty-five percent of ammonia solution and acetic acid (both LC–MS grade) were purchased from Merck. All ISTDs were from Eurisotope. The Strata-X-AW SPE cartridges, 30 mg, 33 µm were bought from Phenomenex.

Preparation of standard solutions

If not stated otherwise, all standards were measured in the matrix obtained after SPE. All stock solutions were stored at −80°C and dilutions were prepared fresh before analysis.

Plant culture

Arabidopsis thaliana plants were grown as previously stated in Niehaus et al. (2020) with slight modifications. Seeds were surface sterilized and cultivated in liquid culture (1.5 mM $MgSO_4 \times 7H_2O$, 1.25 mM KH_2PO_4, 3 mM $CaCl_2$, 18.7 mM KNO_3, 0.1 mM $FeSO_4 \times 7H_2O$, 0.1 mM $Na_2EDTA \times 2H_2O$, 0.13 mM $MnSO_4 \times H_2O$, 0.1 mM H_3BO_3, 30 µM $ZnSO_4 \times 7H_2O$, 1 µM $Na_2MoO_4 \times 2H_2O$, 0.1 µM $CuSO_4 \times 5H_2O$, 0.1 µM $NiCl_2 \times 6H_2O$, 0.125% [w/v] MES, pH 5.7 adjusted with KOH) in a shaker (New Brunswick Innova 42, Eppendorf) with six Sylvania e15t8 tubular fluorescent lamps emitting a photon flux of 45 µmol s^{-1} m^{-2} at 22°C in 100 mL flasks under sterile conditions (10 mg seeds per flask). The shaker was set to 80 rpm. The seedlings were harvested after 7 days. For the 33-day-old plants, Arabidopsis seeds were sown on soil and grown under long-day conditions (Binder KBFW 720 with Osram Lumilux lights,16-h light/8-h darkness, 22°C day, 20°C night, 100 µmol s^{-1} m^{-2} light, and 70% humidity).

T-DNA insertion mutants were obtained from our in-house collection. Their characterization is described in Dahncke and Witte (2013; *gsda*-2, GK432D08), Chen et al. (2016; *cda*-2, SALK036597), and Baccolini and Witte (2019; *nsh1*-1, SALK083120). The genotypes of all mutant lines were confirmed by PCR as described previously (Dahncke and Witte, 2013; Chen et al., 2016). A uniform seed batch was obtained from mutant and wild-type plants grown in parallel in a randomized fashion. The seeds were analyzed 2 weeks post-harvest. For the comparison of mutant seedlings, plants were grown in liquid culture as described above under constant light.

Seeds of asparagus (*Asparagus officinalis* cv. Ramires), barley (*Hordeum vulgare* cv. Golden Promise), common bean (*Phaseolus vulgaris* cv. Black Jamapa), oat (*A. sativa* cv. Fleuron), rice (*O. sativa* cv. Nipponbare), and wheat (*Triticum aestivum* cv. Thatcher) were surface sterilized and cultivated between sheets of filter paper placed in a container filled with some distilled water (Kirchner et al., 2018) and grown in a growth cabinet (Binder KBFW 720 with Osram Lumilux lights) at 22°C, 100 µmol s^{-1} m^{-2} light, and 70% humidity. Whole seedlings were collected 7 days after germination (dag) for all species except *A. officinalis* and *O. sativa* which needed 14 dag to accumulate enough biomass.

The moss *Physcomitrium* (*Physcomitrella*) *patens*, strain Grandsen 2004 (Kamisugi et al., 2008), was cultivated on Knoop medium (250 mg L^{-1} KH_2PO_4, 250 mg L^{-1} KCl, 250 mg L^{-1} $MgSO_4 \times 7H_2O$, 1 g L^{-1} $Ca(NO_3)$, 12.5 mg L^{-1} $FeSO_4 \times 7H_2O$, pH 5.8, and 1.2% [w/v] agar) in a climate chamber under long-day conditions (16-h light/8-h darkness, 22°C day, 20°C night, 100 µmol s^{-1} m^{-2} light, and 70% humidity). Plants were transferred to new plates every 4 weeks during cultivation. Plant material was collected 7 days after transferring to new plates.

Tomato plants (*S. lycopersicum* cv. Micro-Tom) were surface sterilized and transferred to germination medium (0.5 × Murashige and Skoog, 10 g L^{-1} sucrose, and 8 g L^{-1} phyto-agar). The seeds were placed in darkness at room temperature and moved to long-day conditions after 4 days (16-h light/8-h darkness, 22°C day, 20°C night, 100 µmol s^{-1} m^{-2} light, and 70% humidity). Seedlings were harvested 7 dag. Maize (*Zea mays* cv. Rafinio) was grown hydroponically between two plates in tap water wetted foam under long-day conditions (16-h light/8-h darkness, 22°C day, 20°C night, 100 µmol s^{-1} m^{-2} light, and 70% humidity) and harvested 7 dag. *C. reinhardtii* was cultivated for 7 days under the same conditions as the Arabidopsis seeds in liquid culture. *Volvox carteri* was cultivated for 7 days in Fernbach flasks (28°C, 16-h light/8-h dark and 100 µmol s^{-1} m^{-2} light), as described in Klein et al. (2017). *Mougeotia scalaris*

strain SAG 164.80 was cultivated for 7 days (22–25°C, 16-h light/8-h dark, and 46 µmol s^{-1} m^{-2} light), as described in Regensdorff et al. (2018).

All plant and algae material was collected in the middle of the respective light period. Genomic GC-content of respective plant and algae species was acquired from the National Center for Biotechnology Information (NCBI, https://www.ncbi.nlm.nih.gov) or in the case of *M. scalaris* from Regensdorff et al. (2018).

Chromatography and MS parameters

An Agilent 1290 Infinity II LC System coupled with an Agilent 6470 triple quadrupole mass spectrometer was used. Chromatographic separations employed either a 150 × 2.1 mm zic-cHILIC column with 3-µm particle size (Merck) or a 50 × 4.6 mm Hypercarb column with 5-µm particle size (Thermo scientific). The zic-cHILIC column was operated at a flowrate of 0.2 mL min^{-1} and a temperature of 35°C. Mobile phase A was 90% 10 mM ammonium acetate pH 7.7 with 10% acetonitrile and mobile phase B was 10% 2.5 mM ammonium acetate pH 7.7 with 90% acetonitrile. In the following, we refer to chromatographies employing the zic-cHILIC column as cHILIC method. Depending on the analytes, different gradients were used (Tables 7, 8). The Hypercarb column was operated at a flow rate of 0.6 mL min^{-1} and a column temperature of 30°C. Mobile phase A was 5 mM ammonium acetate pH 9.5 and mobile phase B was acetonitrile (for the gradient see Table 9). In the following, we refer to the chromatography using the Hypercarb column as the Hypercarb method. The injection volume was 10 µL and analysis was carried out in positive mode for both methods employing the multiple-reaction-monitoring (MRM) mode. Transitions (precursor ions and product ions) as well as collision energies and fragmentor energies are listed in Supplemental Tables S4–S6. The in-source parameters for the cHILIC method were optimized according to Kong et al. (2018) as a starting point. The following adjustments to fit the plant matrix were made: gas temperature 290°C, gas flow 13 L min^{-1}, nebulizer pressure 25 psi, sheath gas temperature 320°C, sheath gas flow 11 L min^{-1}, capillary voltage 2,500 V, and nozzle voltage 2,000 V. The optimized in-source parameters for the Hypercarb method were: gas temperature 250°C, gas flow 12 L min^{-1}, nebulizer pressure 20 psi, sheath gas temperature 395°C, sheath gas flow 12 L min^{-1}, capillary voltage 3,000 V, and nozzle voltage 500 V. For the determination of exact masses, samples were separated with a Vanquish LC (Thermo Fisher) by the Hypercarb method. The metabolites were analyzed with an Orbitrap Q Exactive Plus mass spectrometer (Thermo Fisher) at a resolution of 70,000 when operated in full MS mode or 17,500 for detection of product ions in PRM (parallel reaction monitoring) mode with 35-V normalized collision energy or 140,000 using single-ion monitoring (SIM) in the positive polarity mode. Automatic gain control (AGC) target and maximum injection time were set to $3e^6$ and 200 ms, respectively. The heated ESI (electrospray-ionization) source was operated at 0-eV collision-induced dissociation (CID), sheath gas flow 45, auxiliary gas flow 10, sweep gas flow 2, spray voltage 3.5 kV, capillary temperature 250°C, S-lens RF level 45.0, and aux gas heater 400°C. All reported values were obtained with the Freestyle software (ver. 1.5, Thermo Fisher). For UV detection, samples were prepared as described in the respective section and identical to the procedure described for the analysis of the MEF. The detector was a VF-D40-A variable wavelength detector set to 254 nm. Identity of peaks was confirmed by MS as described before with an orbitrap mass analyzer in full MS mode.

Table 7 Gradient for NT chromatography on the zic-cHILIC column

Time (min)	Mobile phase A (%)	Mobile phase B (%)
0.0	20.0	80.0
7.0	20.0	80.0
12.0	40.0	60.0
17.0	40.0	60.0
19.0	20.0	80.0
23.0	20.0	80.0

Table 8 Gradient for nucleoside chromatography on the zic-cHILIC column

Time (min)	Mobile phase A (%)	Mobile phase B (%)
0.0	10.0	90.0
7.0	10.0	90.0
12.0	40.0	60.0
17.0	40.0	60.0
19.0	10.0	90.0
23.0	10.0	90.0

Table 9 Gradient for NT chromatography on the Hypercarb column

Time (min)	Mobile phase A (%)	Mobile phase B (%)
0.0	96.0	4.0
10.0	70.0	30.0
10.10	0.0	100.0
11.50	0.0	100.0
11.60	96.0	4.0
20.0	96.0	4.0

Sample preparation and SPE

Plant samples were harvested, briefly washed in tap water, and dried thoroughly with a paper towel. Approximately 100-mg plant material was weighed into a 2-mL safe-lock centrifuge-vial and frozen in liquid nitrogen together with five 5-mm steel beads (one 7-mm steel bead and five 5-mm steel beads in case of seeds). The exact sample weight was noted and used for calculating analyte concentrations. The tissue was disrupted using a MM 400 beadmill (Retsch, Germany) at 28 Hz for 2.30 min. Onto the frozen powder, 1 mL of ice-cold 15% TCA solution was added including the respective isotope standards. The samples were briefly vortexed, ground once more at 28 Hz for 2.30 min, and then centrifuged for 10 min at 4°C at 40,000 × *g*. To the supernatant 1 mL 78/22 DCM/TOA was added. Samples were vortexed for 12 s and centrifuged for 2 min at 4°C and 5,000 × *g*. The upper phase from each sample was transferred to a new tube and 1 mL water as well as 5 µL 0.5%

acetic acid were added. This mixture was applied to a 30 mg/1 mL Strata X-AW cartridge that had been equilibrated sequentially with 1 mL methanol, 1 mL 2/25/73 formic acid/methanol/H_2O, and 1 mL 10 mM ammonium acetate pH 4.5. The sample solution was allowed to enter the cartridge for 2 min without suction and then percolated through the solid phase at a flowrate of about 1 mL min^{-1} using a vacuum manifold. The flow-through containing the nucleoside fraction was collected and evaporated in an Alpha 1–2 LDplus freeze dryer (Christ, Germany). The SPE cartridge was washed with 1 mL 1-mM ammonium acetate pH 4.5 and 1 mL methanol, dried shortly, and eluted two times with 0.5 mL 20/80 ammonia/methanol. The eluate was dried in a vacuum concentrator until no liquid was left. For the cHILIC method, the samples were reconstituted in 50 µL 30/9/1 acetonitrile/water/100 mM ammonium acetate pH 7.7. For the Hypercarb method, the samples were reconstituted in 50 µL 95/5 of 5-mM ammonium acetate (pH 9.5)/acetonitrile.

Method validation

We analyzed the developed method in terms of linearity, precision, LLOQ, relative recovery, and matrix effects. For calibration curves, peak area sums of ISTDs were plotted against their concentration. Concentrations were chosen in a range relevant in biological samples. Intra-day precision was calculated using the peak area sums of different concentrations of ISTDs in SPE-matrix, injecting the same sample three times a day. The inter-day precision was calculated using the peak area sums of different concentrations of ISTDs in SPE-matrix that have been injected on 3 days consecutively. Samples were stored at 4°C. The LLOQ was defined as the lowest concentrated standard with acceptable peak shape. The relative recovery was calculated as following:

$$\frac{\text{area of isotope standard added to extraction buffer}}{\text{area of isotope standard added after SPE}} \times 100 = \text{relative recovery } (\%).$$

The matrix effect was determined by comparing ISTDs with the same concentration separated either by the cHILIC method or the Hypercarb method in (i) matrix after extracting the TCA with the DCM/TOA, (ii) in matrix after the SPE procedure, and (iii) in pure buffer (for the cHILIC method 30/9/1 acetonitrile/water/100 mM ammonium acetate pH 7.7 and for the Hypercarb method 95/5 of 5-mM ammonium acetate [pH 9.5]/acetonitrile). The MEF was calculated according to Zhou et al. (2017):

$$\frac{\text{average area ISTD in buffer} - \text{average area of ISTD in matrix}}{\text{average area of ISTD in buffer}} \times 100 = \text{MEF}.$$

Quantification of metabolites

The amount of metabolites in plant samples was calculated either by the isotope dilution technique or with external calibration curves in SPE-matrix. ISTDs were added to the extraction buffer prior to extraction. Only calibration curves with a coefficient of determination (R^2) $>$ 0.99 were accepted.

Calculation of concentrations of metabolites in plant cell compartments

To determine the concentrations of rNTPs and dNTPs per unit NT-containing cell volume, we used the calculations of Koffler et al. (2013). They determined the total volume of the mesophyll cells in four sections of an Arabidopsis leaf and the volumes of the individual subcellular compartments in these sections. We grew plants until the leaves met the morphological criteria stated by Koffler and colleagues, i.e. to a size of approximately 1.5 × 3.0 cm, and then extracted them. We determined an average (i.e. not in sections but for the whole) leaf mesophyll volume per unit total fresh weight (AMV) of 600.0 µL g^{-1} fresh weight. We assumed that the nucleus, the cytoplasm, the mitochondria, and the plastids contain NTs (these are NT-containing compartments, NCC), whereas other cell compartments are likely devoid of relevant concentrations of NTs. An average of the percentile volumes of the compartments was calculated. Together, the NCCs accounted for 26.86% of the total mesophyll volume. We then calculated the concentrations of dNTPs and rNTPs in the NCC (Y in the formula), while X is the amount of metabolite in pmol g^{-1} fresh weight that was measured:

$$\frac{X\left[\frac{\text{pmol}}{\text{g}}\right]}{\text{AVM}\left[\frac{\mu\text{l}}{\text{g}}\right]} \times \frac{100\%}{26.86\%} = Y\ [\mu\text{M}].$$

Statistical analysis

Statistical analysis was performed using Prism 8 software. One-way analysis of variance (ANOVA) with Tukey's post test or two-way ANOVA with Sidak's post test were used. Different letters or a star indicate differences at significance level of $P < 0.5$. Statistical analysis results are shown in Supplemental File S1.

Accession numbers

Information regarding used mutants can be found in the GenBank/EMBL data libraries under the following accession numbers: *cda* (At2g19570), *gsda* (At5g28050), *nsh1* (At2g36310).

Supplemental data

Supplemental Figure S1. Chromatograms of all analyzed NTs by hypercarb chromatography.

Supplemental Figure S2. Chromatograms of all analyzed NTs by cHILIC chromatography.

Supplemental Figure S3. Chromatograms of all analyzed Ns by cHILIC chromatography.

Supplemental Figure S4. Analysis of NTs in Arabidopsis leaves by HPLC and UV detection.

Supplemental Figure S5. SPE enables detection of dNTPs in several plant and algae species.

Supplemental Figure S6. SPE enables detection of rNs in Arabidopsis seeds and seedlings.

Supplemental Table S1. Literature survey on NT analysis in plants

Supplemental Table S2. Tested conditions for SPE optimization

Supplemental Table S3. Relative recovery of metabolites extracted by different methods.

Supplemental Table S4. Precursor, transitions (quantifier, qualifier), fragmentor, collision energy and retention times for NTP measurements

Supplemental Table S5. Precursor, transitions (quantifier, qualifier), fragmentor energy, collision energy and retention times for **NMP** measurements

Supplemental Table S6. Precursor, transitions (quantifier, qualifier), fragmentor energy, collision energy and retention times for nucleoside measurements

Supplemental Table S7. Intra-day variation and inter-day variation for different concentrations of NTs seperated by the Hypercarb or cHILIC method

Supplemental Table S8. Intra-day variation and inter-day variation for different concentrations of Ns seperated by the cHILIC method

Supplemental Table S9. Determination of MEF at 5- and 50-pmol dNTP and rNTP ISTDs, respectively, on column

Supplemental Table S10. Determination of MEF at 5-pmol nucleoside ISTD on column

Supplemental Table S11. NTPs analyzed with an Orbitrap mass spectrometer

Supplemental File S1. ANOVA tables.

Acknowledgments

The authors like to express their gratitude to Andreas Fricke, Jannis Rinne, Mareike Schallenberg-Rüdinger, Jennifer Senkler, and Jana Streubel for providing plant material and seeds and André Specht for technical assistance regarding LC and MS. They are very grateful to Henrik Buschmann, Armin Hallmann, and Benjamin Klein for growing and providing algae. They also like to thank Bernd Thierfelder and Chi Vinh Duong (Phenomenex) and Sascha Beutel for helpful discussion regarding sample preparation.

Funding

This work was supported by the Deutsche Forschungsgemeinschaft (grant no. HE 5949/3-1 to M.H.), (grant no. WI3411/4-1 to C-P.W.), and (grant no. INST 187/741-1 FUGG).

Conflict of interest statement. None declared.

References

Aoyagi S, Sugiyama M, Fukuda H (1998) BEN1 and ZEN1 cDNAs encoding S1-type DNases that are associated with programmed cell death in plants. FEBS Lett **429**: 134–138

Ashihara H, Crozier A, Ludwig IA (2020) Plant Nucleotide Metabolism: Biosynthesis, Degradation, and Alkaloid Formation. Wiley Blackwell, Chichester

Ashihara H, Mitsui K, Ukaji T (1987) A simple analysis of purine and pyrimidine nucleotides in plant cells by high-performance liquid chromatography. Z Naturforsch C **42**: 297–299

Assmann SM (2002) Heterotrimeric and unconventional GTP binding proteins in plant cell signaling. Plant Cell **14**: S355–S373

Baccolini C, Witte C-P (2019) AMP and GMP catabolism in arabidopsis converge on Xanthosine, which is degraded by a nucleoside hydrolase heterocomplex. Plant Cell **31**: 734–751

Berglund A-K, Navarrete C, Engqvist MKM, Hoberg E, Szilagyi Z, Taylor RW, Gustafsson CM, Falkenberg M, Clausen AR (2017) Nucleotide pools dictate the identity and frequency of ribonucleotide incorporation in mitochondrial DNA. PLoS Genet **13**: e1006628

Bieleski RL (1964) The problem of halting enzyme action when extracting plant tissues. Anal Biochem **9**: 431–442

Bieleski RL, Young RE (1963) Extraction and separation of phosphate esters from plant tissues. Anal Biochem **6**: 54–68

Buckland RJ, Watt DL, Chittoor B, Nilsson AK, Kunkel TA, Chabes A (2014) Increased and imbalanced dNTP pools symmetrically promote both leading and lagging strand replication infidelity. PLoS Genet **10**: e1004846

Burdett H, Bentham AR, Williams SJ, Dodds PN, Anderson PA, Banfield MJ, Kobe B (2019) The plant "resistosome": structural insights into immune signaling. Cell Host Microbe **26**: 193–201

Carrari F, Coll-Garcia D, Schauer N, Lytovchenko A, Palacios-Rojas N, Balbo I, Rosso M, Fernie AR (2005) Deficiency of a plastidial adenylate kinase in Arabidopsis results in elevated photosynthetic amino acid biosynthesis and enhanced growth. Plant Physiol **137**: 70–82

Castroviejo M, Tharaud D, Mocquot B, Litvak S (1979) Factors affecting the onset of deoxyribonucleic acid synthesis during wheat embryo germination: study of the changes in DNA polymerases A, B and C and the pool of DNA precursors. Biochem J **181**: 193–199

Chabosseau P, Buhagiar-Labarchède G, Onclercq-Delic R, Lambert S, Debatisse M, Brison O, Amor-Guéret M (2011) Pyrimidine pool imbalance induced by BLM helicase deficiency contributes to genetic instability in Bloom syndrome. Nat Commun **2**: 368

Chen M, Herde M, Witte C-P (2016) Of the nine cytidine deaminase-like genes in arabidopsis, eight are pseudogenes and only one is required to maintain pyrimidine homeostasis in vivo. Plant Physiol **171**: 799–809

Chen M, Urs MJ, Sánchez-González I, Olayioye MA, Herde M, Witte C-P (2018) m6A RNA degradation products are catabolized by an evolutionarily conserved N6-methyl-AMP deaminase in plant and mammalian cells. Plant Cell **30**: 1511–1522

Chen M, Witte C-P (2020) A kinase and a glycosylase catabolize pseudouridine in the peroxisome to prevent toxic pseudouridine monophosphate accumulation. Plant Cell **32**: 722–739

Clausen AR, Girandon L, Ali A, Knecht W, Rozpedowska E, Sandrini MPB, Andreasson E, Munch-Petersen B, Piškur J (2012) Two thymidine kinases and one multisubstrate deoxyribonucleoside kinase salvage DNA precursors in *Arabidopsis thaliana*. FEBS J **279**: 3889–3897

Cohen S, Megherbi M, Jordheim LP, Lefebvre I, Perigaud C, Dumontet C, Guitton J (2009) Simultaneous analysis of eight nucleoside triphosphates in cell lines by liquid chromatography coupled with tandem mass spectrometry. J Chromatogr B **877**: 3831–3840

Dahncke K, Witte C-P (2013) Plant purine nucleoside catabolism employs a guanosine deaminase required for the generation of xanthosine in Arabidopsis. Plant Cell **25**: 4101–4109

Dietmair S, Timmins NE, Gray PP, Nielsen LK, Krömer JO (2010) Towards quantitative metabolomics of mammalian cells:

development of a metabolite extraction protocol. Anal Biochem **404**: 155–164

Dubois E, Córdoba-Cañero D, Massot S, Siaud N, Gakière B, Domenichini S, Guérard F, Roldan-Arjona T, Doutriaux M-P (2011) Homologous recombination is stimulated by a decrease in dUTPase in Arabidopsis. PLoS ONE **6**: e18658

Dutta I, Dutta PK, Smith DW, O'Donovan GA (1991) High-performance liquid chromatography of deoxyribonucleoside di- and triphosphates in tomato roots. J Chromatogr A **536**: 237–243

Faivre-Nitschke SE, Grienenberger JM, Gualberto JM (1999) A prokaryotic-type cytidine deaminase from *Arabidopsis thaliana* gene expression and functional characterization. Eur J Biochem **263**: 896–903

Farrow SC, Emery RN (2012) Concurrent profiling of indole-3-acetic acid, abscisic acid, and cytokinins and structurally related purines by high-performance-liquid-chromatography tandem electrospray mass spectrometry. Plant Methods **8**: 42

Feller W, Schimpf-Weiland G, Follmann H (1980) Deoxyribonucleotide biosynthesis in synchronous algae cells. Eur J Biochem **110**: 85–92

Frydman RB, Neufeld EF, Hassid WZ (1963) Thymidine diphosphate d-galactose pyrophosphorylase of *Phaseolus aureus*. Biochim Biophys Acta **77**: 332–334

Galmarini CM, Jordheim L, Dumontet C (2003) Pyrimidine nucleoside analogs in cancer treatment. Exp Rev Anticancer Ther **3**: 717–728

Garton S, Knight H, Warren GJ, Knight MR, Thorlby GJ (2007) Crinkled leaves 8—a mutation in the large subunit of ribonucleotide reductase—leads to defects in leaf development and chloroplast division in *Arabidopsis thaliana*. Plant J Cell Mol Biol **50**: 118–127

Gon S, Napolitano R, Rocha W, Coulon S, Fuchs RP (2011) Increase in dNTP pool size during the DNA damage response plays a key role in spontaneous and induced-mutagenesis in *Escherichia coli*. Proc Natl Acad Sci U S A **108**: 19311–19316

Greilhuber J, Dolezel J, Leitch IJ (2012) Plant Genomes, Their Residents, and Their Evolutionary Dynamics, Springer, Wien

Guérard F, Pétriacq P, Gakière B, Tcherkez G (2011) Liquid chromatography/time-of-flight mass spectrometry for the analysis of plant samples: a method for simultaneous screening of common cofactors or nucleotides and application to an engineered plant line. Plant Physiol Biochem **49**: 1117–1125

Guo S, Duan J-A, Qian D, Wang H, Tang Y, Qian Y, Wu D, Su S, Shang E (2013) Hydrophilic interaction ultra-high performance liquid chromatography coupled with triple quadrupole mass spectrometry for determination of nucleotides, nucleosides and nucleobases in *Ziziphus* plants. J Chromatogr A, **1301**: 147–155

Harmenberg J, Karlsson AHJ, Gilljam G (1987) Comparison of sample preparation methods for the high-performance liquid chromatographic analysis of cell culture extracts for triphosphate ribonucleosides and deoxyribonucleosides. Anal Biochem **161**: 26–31

Henneré G, Becher F, Pruvost A, Goujard C, Grassi J, Benech H (2003) Liquid chromatography–tandem mass spectrometry assays for intracellular deoxyribonucleotide triphosphate competitors of nucleoside antiretrovirals. J Chromatogr B **789**: 273–281

Ikuma H, Tetley RM (1976) Possible interference by an acid-stable enzyme during the extraction of nucleoside di- and triphosphates from higher plant tissues. Plant Physiol **58**: 320–323

Johnston CA, Taylor JP, Gao Y, Kimple AJ, Grigston JC, Chen J-G, Siderovski DP, Jones AM, Willard FS (2007) GTPase acceleration as the rate-limiting step in Arabidopsis G protein-coupled sugar signaling. Proc Natl Acad Sci U S A **104**: 17317–17322

Jung B, Flörchinger M, Kunz H-H, Traub M, Wartenberg R, Jeblick W, Neuhaus HE, Möhlmann T (2009) Uridine-ribohydrolase is a key regulator in the uridine degradation pathway of Arabidopsis. Plant Cell **21**: 876–891

Jung B, Hoffmann C, Möhlmann T (2011) Arabidopsis nucleoside hydrolases involved in intracellular and extracellular degradation of purines. Plant J Cell Mol Biol **65**: 703–711

Kafer C, Thornburg RW (2000) *Arabidopsis thaliana* cytidine deaminase 1 shows more similarity to prokaryotic enzymes than to eukaryotic enzymes. J Plant Biol **43**: 162–170

Kamisugi Y, von Stackelberg M, Lang D, Care M, Reski R, Rensing SA, Cuming AC (2008) A sequence-anchored genetic linkage map for the moss, *Physcomitrella patens*. Plant J Cell Mol Biol **56**: 855–866

Katahira R, Ashihara H (2006) Role of adenosine salvage in wound-induced adenylate biosynthesis in potato tuber slices. Plant Physiol Biochem **44**: 551–555

Katan R, Avigad G (1966) NADP dependent oxidation of TDP-glucose by an enzyme system from sugar beets. Biochem Biophys Res Commun **24**: 18–24

Kazibwe Z, Soto-Burgos J, MacIntosh GC, Bassham DC (2020) TOR mediates the autophagy response to altered nucleotide homeostasis in a ribonuclease mutant. J Exp Bot eraa410

Khym JX (1975) An analytical system for rapid separation of tissue nucleotides at low pressures. Clin Chem **21**: 1245–1252

Kirchner TW, Niehaus M, Rössig KL, Lauterbach T, Herde M, Küster H, Schenk MK (2018) Molecular background of pi deficiency-induced root hair growth in *Brassica carinata*—a fasciclin-like arabinogalactan protein is involved. Front Plant Sci **9**: 1372

Klein B, Wibberg D, Hallmann A (2017) Whole transcriptome RNA-Seq analysis reveals extensive cell type-specific compartmentalization in *Volvox carteri*. BMC Biol **15**: 1–22

Koffler BE, Bloem E, Zellnig G, Zechmann B (2013) High resolution imaging of subcellular glutathione concentrations by quantitative immunoelectron microscopy in different leaf areas of Arabidopsis. Micron **45**: 119–128

Kong Z, Jia S, Chabes AL, Appelblad P, Lundmark R, Moritz T, Chabes A (2018) Simultaneous determination of ribonucleoside and deoxyribonucleoside triphosphates in biological samples by hydrophilic interaction liquid chromatography coupled with tandem mass spectrometry. Nucl Acids Res **46**: e66

Kopecná M, Blaschke H, Kopecny D, Vigouroux A, Koncitíková R, Novák O, Kotland O, Strnad M, Moréra S, von Schwartzenberg K (2013) Structure and function of nucleoside hydrolases from *Physcomitrella patens* and maize catalyzing the hydrolysis of purine, pyrimidine, and cytokinin ribosides. Plant Physiol **163**: 1568–1583

Kumar D, Abdulovic AL, Viberg J, Nilsson AK, Kunkel TA, Chabes A (2011) Mechanisms of mutagenesis in vivo due to imbalanced dNTP pools. Nucl Acids Res **39**: 1360–1371

Kuskovsky R, Buj R, Xu P, Hofbauer S, Doan MT, Jiang H, Bostwick A, Mesaros C, Aird KM, Snyder NW (2019) Simultaneous isotope dilution quantification and metabolic tracing of deoxyribonucleotides by liquid chromatography high resolution mass spectrometry. Anal Biochem **568**: 65–72

Le Ret M, Belcher S, Graindorge S, Wallet C, Koechler S, Erhardt M, Williams-Carrier R, Barkan A, Gualberto JM (2018) Efficient replication of the plastid genome requires an organellar thymidine kinase. Plant Physiol **178**: 1643–1656

Lee HO, Davidson JM, Duronio RJ (2009) Endoreplication: polyploidy with purpose. Genes Dev **23**: 2461–2477

Leija C, Rijo-Ferreira F, Kinch LN, Grishin NV, Nischan N, Kohler JJ, Hu Z, Phillips MA (2016) Pyrimidine salvage enzymes are essential for de novo biosynthesis of deoxypyrimidine nucleotides in *Trypanosoma brucei*. PLoS Pathogens **12**: e1006010

Leiva-Neto JT, Grafi G, Sabelli PA, Dante RA, Woo Y-M, Maddock S, Gordon-Kamm WJ, Larkins BA (2004) A dominant negative mutant of cyclin-dependent kinase A reduces endoreduplication but not cell size or gene expression in maize endosperm. Plant Cell **16**: 1854–1869

Liu B, Winkler F, Herde M, Witte C-P, Großhans J (2019) A Link between deoxyribonucleotide metabolites and embryonic cell-cycle control. Curr Biol **29**: 1187–1192.e3

de Lorenzo V (2014) From the selfish gene to selfish metabolism: revisiting the central dogma. BioEssays **36**: 226–235

Meyer R, Wagner KG (1985) Determination of nucleotide pools in plant tissue by high-performance liquid chromatography. Anal Biochem **148**: 269–276

Neufeld EF (1962) Formation and epimerization of dTDP-D-galactose catalyzed by plant enzymes. Biochem Biophys Res Commun **7**: 461–466

Nick McElhinny SA, Kumar D, Clark AB, Watt DL, Watts BE, Lundström E-B, Johansson E, Chabes A, Kunkel TA (2010a) Genome instability due to ribonucleotide incorporation into DNA. Nat Chem Biol **6**: 774–781

Nick McElhinny SA, Watts BE, Kumar D, Watt DL, Lundström E-B, Burgers PMJ, Johansson E, Chabes A, Kunkel TA (2010b) Abundant ribonucleotide incorporation into DNA by yeast replicative polymerases. Proc Natl Acad Sci U S A **107**: 4949–4954

Niehaus M, Straube H, Künzler P, Rugen N, Hegermann J, Giavalisco P, Eubel H, Witte C-P, Herde M (2020) Rapid affinity purification of tagged plant mitochondria (Mito-AP) for metabolome and proteome analyses. Plant Physiol **182**: 1194–1210

Nieman RH, Pap DL, Clark RA (1978) Rapid purification of plant nucleotide extracts with xad-2, polyvinylpolypyrrolidone and charcoal. J Chromatogr A **161**: 137–146

Nizam S, Qiang X, Wawra S, Nostadt R, Getzke F, Schwanke F, Dreyer I, Langen G, Zuccaro A (2019) *Serendipita indica* E5′NT modulates extracellular nucleotide levels in the plant apoplast and affects fungal colonization. EMBO Rep **20**

Nordlund P, Reichard P (2006) Ribonucleotide reductases. Annu Rev Biochem **75**: 681–706

Nygaard P (1972) Deoxyribonucleotide pools in plant tissue cultures. Physiol Plant **26**: 29–33

Odmark G, Kihlman BA (1965) Effects of chromosome-breaking purine derivatives on nucleic acid synthesis and on the levels of adenosine 5′-triphosphate and deoxyadenosine 5′-triphosphate in bean root tips. Mutat Res **2**: 274–286

Pabst M, Grass J, Fischl R, Léonard R, Jin C, Hinterkörner G, Borth N, Altmann F (2010) Nucleotide and nucleotide sugar analysis by liquid chromatography–electrospray ionization–mass spectrometry on surface-conditioned porous graphitic carbon. Anal Chem **82**: 9782–9788

Pedroza-García JA, Nájera-Martínez M, de La Paz Sanchez M, Plasencia J (2015) *Arabidopsis thaliana* thymidine kinase 1a is ubiquitously expressed during development and contributes to confer tolerance to genotoxic stress. Plant Mol Biol **87**: 303–315

Pedroza-García J-A, Nájera-Martínez M, Mazubert C, Aguilera-Alvarado P, Drouin-Wahbi J, Sánchez-Nieto S, Gualberto JM, Raynaud C, Plasencia J (2019) Role of pyrimidine salvage pathway in the maintenance of organellar and nuclear genome integrity. Plant J Cell Mol Biol **97**: 430–446

Rampazzo C, Miazzi C, Franzolin E, Pontarin G, Ferraro P, Frangini M, Reichard P, Bianchi V (2010) Regulation by degradation, a cellular defense against deoxyribonucleotide pool imbalances. Mutat Res **703**: 2–10

Raveneau M-P, Benamar A, Macherel D (2017) Water content, adenylate kinase, and mitochondria drive adenylate balance in dehydrating and imbibing seeds. J Exp Bot **68**: 3501–3512

Regensdorff M, Deckena M, Stein M, Borchers A, Scherer G, Lammers M, Hänsch R, Zachgo S, Buschmann H (2018) Transient genetic transformation of *Mougeotia scalaris* (Zygnematophyceae) mediated by the endogenous α-tubulin1 promoter. J Phycol **54**: 840–849

Riegler H, Geserick C, Zrenner R (2011) *Arabidopsis thaliana* nucleosidase mutants provide new insights into nucleoside degradation. New Phytol **191**: 349–359

Riondet C, Morel S, Alcaraz G (2005) Determination of total ribonucleotide pool in plant materials by high-pH anion-exchange high-performance liquid chromatography following extraction with potassium hydroxide. J Chromatogr A **1077**: 120–127

Robak P, Robak T (2013) Older and new purine nucleoside analogs for patients with acute leukemias. Cancer Treat Rev **39**: 851–861

Rolletschek H, Melkus G, Grafahrend-Belau E, Fuchs J, Heinzel N, Schreiber F, Jakob PM, Borisjuk L (2011) Combined noninvasive imaging and modeling approaches reveal metabolic compartmentation in the barley endosperm. Plant Cell **23**: 3041–3054

Sabina RL, Paul A-L, Ferl RJ, Laber B, Lindell SD (2007) Adenine nucleotide pool perturbation is a metabolic trigger for AMP deaminase inhibitor-based herbicide toxicity. Plant Physiol **143**: 1752–1760

Sakamoto W, Takami T (2014) Nucleases in higher plants and their possible involvement in DNA degradation during leaf senescence. J Exp Bot **65**: 3835–3843

Salem SA, Yoshida T, Perez de Souza L, Alseekh S, Bajdzienko K, Fernie AR, Giavalisco P (2020) An improved extraction method enables the comprehensive analysis of lipids, proteins, metabolites and phytohormones from a single sample of leaf tissue under water-deficit stress. Plant J **103**: 1614–1632

Savitch LV, Barker-Åstrom J, Ivanov AG, Hurry V, Öquist G, Huner NP, Gardeström P (2001) Cold acclimation of *Arabidopsis thaliana* results in incomplete recovery of photosynthetic capacity, associated with an increased reduction of the chloroplast stroma. Planta **214**: 295–303

Sawert A, Backer A, Plank-Schumacher K-H, Wagner KG (1987) Determination of nucleotides and nucleosides in cereal leaves by high performance liquid chromatography. J Plant Physiol **127**: 183–186

Schroeder RY, Zhu A, Eubel H, Dahncke K, Witte C-P (2018) The ribokinases of *Arabidopsis thaliana* and *Saccharomyces cerevisiae* are required for ribose recycling from nucleotide catabolism, which in plants is not essential to survive prolonged dark stress. New Phytol **217**: 233–244

Šmarda P, Bureš P, Horová L, Leitch IJ, Mucina L, Pacini E, Tichý L, Grulich V, Rotreklová O (2014) Ecological and evolutionary significance of genomic GC content diversity in monocots. Proc Natl Acad Sci U S A **111**: E4096–E4102

de Souza AP, Cocuron J-C, Garcia AC, Alonso AP, Buckeridge MS (2015) Changes in whole-plant metabolism during the grain-filling stage in sorghum grown under elevated CO_2 and drought. Plant Physiol **169**: 1755–1765

Stasolla C, Katahira R, Thorpe TA, Ashihara H (2003) Purine and pyrimidine nucleotide metabolism in higher plants. J Plant Physiol **160**: 1271–1295

Stitt M, Lilley RM, Heldt HW (1982) Adenine nucleotide levels in the cytosol, chloroplasts, and mitochondria of wheat leaf protoplasts. Plant Physiol **70**: 971–977

Tanaka K, Yoshioka A, Tanaka S, Wataya Y (1984) An improved method for the quantitative determination of deoxyribonucleoside triphosphates in cell extracts. Anal Biochem **139**: 35–41

Traub M, Flörchinger M, Piecuch J, Kunz H-H, Weise-Steinmetz A, Deitmer JW, Ekkehard Neuhaus H, Möhlmann T (2007). The fluorouridine insensitive 1 (fur1) mutant is defective in equilibrative nucleoside transporter 3 (ENT3), and thus represents an important pyrimidine nucleoside uptake system in *Arabidopsis thaliana*. Plant J Cell Mol Biol **49**: 855–864

Ullrich J, Calvin M (1962) Alcohol-resistant phosphatase activity in chloroplasts. Biochim Biophys Acta **63**: 1–10

Vetsigian K, Goldenfeld N (2008) Genome rhetoric and the emergence of compositional bias. Proc Natl Acad Sci U S A **106**: 215–220

Vincenzetti S, Cambi A, Neuhard J, Schnorr K, Grelloni M, Vita A (1999) Cloning, expression, and purification of cytidine deaminase from *Arabidopsis thaliana*. Protein Expr Purif **15**: 8–15

Wang C, Liu Z (2006) Arabidopsis ribonucleotide reductases are critical for cell cycle progression, DNA damage repair, and plant development. Plant Cell **18**: 350–365

Wang M, Oppedijk BJ, Caspers MPM, Lamers GEM, Boot MJ, Geerlings DNG, Bakhuizen B, Meijer AH, Duijn BV (1998) Spatial and temporal regulation of DNA fragmentation in the aleurone of germinating barley. J Exp Bot **49**: 1293–1301

Werner AK, Romeis T, Witte C-P (2010) Ureide catabolism in *Arabidopsis thaliana* and Escherichia coli. Nat Chem Biol **6**: 19–21

Werner AK, Witte C-P (2011) The biochemistry of nitrogen mobilization: purine ring catabolism. Trends Plant Sci **16**: 381–387

Witte C-P, Herde M (2020) Nucleotide metabolism in plants. Plant Physiol **182**: 63–78

Xu D, Leister D, Kleine T (2020) VENOSA4, a human dNTPase SAMHD1 homolog, contributes to chloroplast development and abiotic stress tolerance. Plant Physiol **182**: 721–729

Xu J, Zhang L, Yang D-L, Li Q, He Z (2015) Thymidine kinases share a conserved function for nucleotide salvage and play an essential role in *Arabidopsis thaliana* growth and development. New Phytol **208**: 1089–1103

Yabuki N, Ashihara H (1991) Catabolism of adenine nucleotides in suspension-cultured plant cells. Biochim Biophys Acta **1073**: 474–480

Yoo S-C, Cho S-H, Sugimoto H, Li J, Kusumi K, Koh H-J, Iba K, Paek N-C (2009) Rice virescent3 and stripe1 encoding the large and small subunits of ribonucleotide reductase are required for chloroplast biogenesis during early leaf development. Plant Physiol **150**: 388–401

Zhou W, Yang S, Wang PG (2017) Matrix effects and application of matrix effect factor. Bioanalysis **9**: 1839–1844

Zrenner R, Stitt M, Sonnewald U, Boldt R (2006) Pyrimidine and purine biosynthesis and degradation in plants. Annu Rev Plant Biol **57**: 805–836